Volume 12
Number 11
7 June 2024
Pages 2759-2994

Biomaterials Science

rsc.li/biomaterials-science

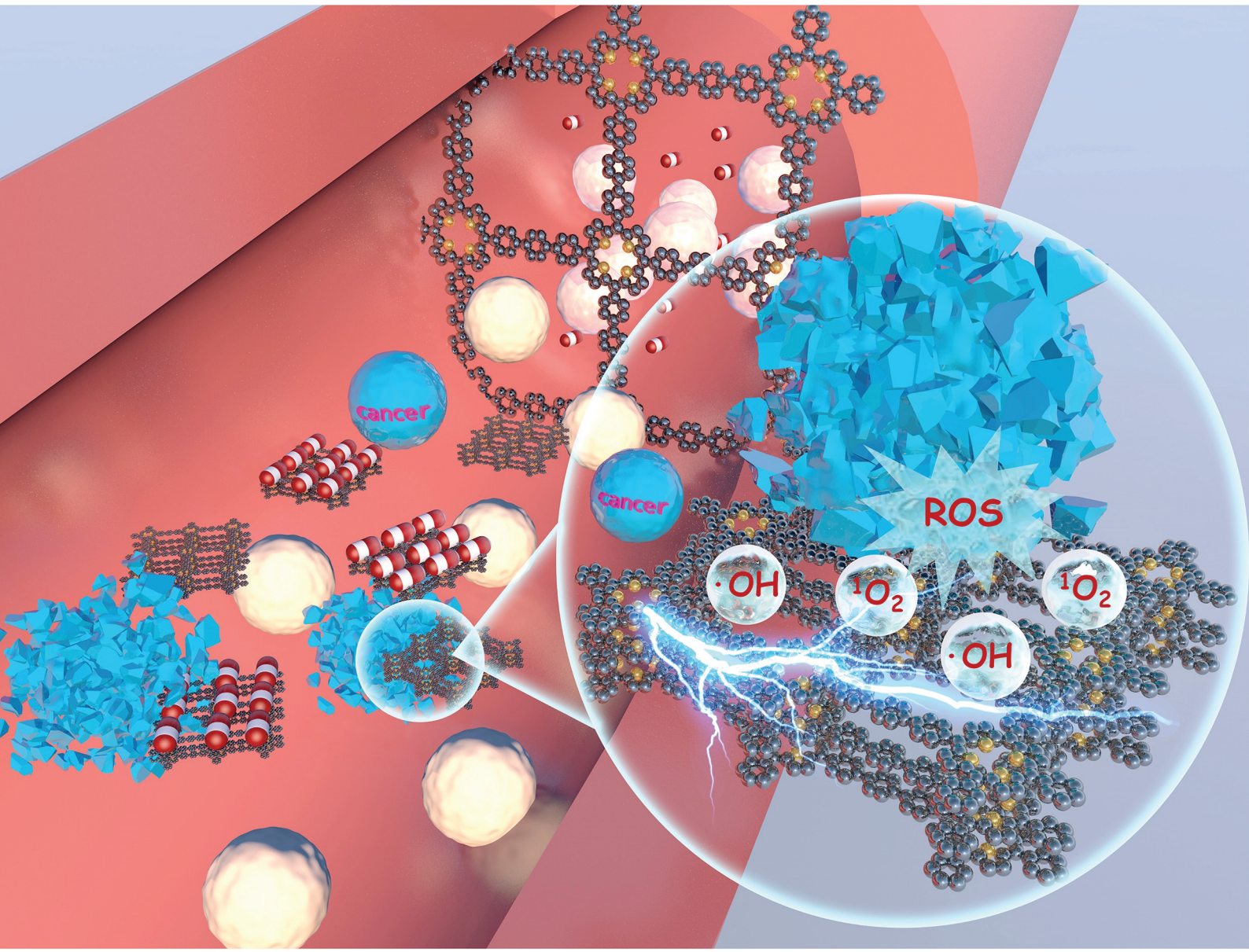

ISSN 2047-4849

ROYAL SOCIETY OF CHEMISTRY

REVIEW ARTICLE
Jie Zheng, Jie Ma *et al.*
Porphyrin-based covalent organic frameworks from design, synthesis to biological applications

European Society for Biomaterials

Biomaterials Science

ROYAL SOCIETY OF CHEMISTRY

REVIEW

View Article Online
View Journal | View Issue

Cite this: *Biomater. Sci.*, 2024, **12**, 2766

Porphyrin-based covalent organic frameworks from design, synthesis to biological applications

Xin-Gui Li,†[a] Junjian Li,†[a] JinFeng Chen,[a] Liangmei Rao,[a] Libin Zheng,[a] Fei Yu,[c] Yijing Tang,[d] Jie Zheng *[d] and Jie Ma *[a,b]

Received 8th February 2024,
Accepted 15th April 2024

DOI: 10.1039/d4bm00214h

rsc.li/biomaterials-science

Covalent organic frameworks (COFs) constitute a class of highly functional porous materials composed of lightweight elements interconnected by covalent bonds, characterized by structural order, high crystallinity, and large specific surface area. The integration of naturally occurring porphyrin molecules, renowned for their inherent rigidity and conjugate planarity, as building blocks in COFs has garnered significant attention. This strategic incorporation addresses the limitations associated with free-standing porphyrins, resulting in the creation of well-organized porous crystal structures with molecular-level directional arrangements. The unique optical, electrical, and biochemical properties inherent to porphyrin molecules endow these COFs with diversified applications, particularly in the realm of biology. This review comprehensively explores the synthesis and modulation strategies employed in the development of porphyrin-based COFs and delves into their multifaceted applications in biological contexts. A chronological depiction of the evolution from design to application is presented, accompanied by an analysis of the existing challenges. Furthermore, this review offers directional guidance for the structural design of porphyrin-based COFs and underscores their promising prospects in the field of biology.

1. Introduction

Porphyrins, pervasive in nature, constitute crucial components in various living organisms, including cytochromes, hemoglobin, and chlorophyll. These biological entities consist of metalloporphyrin complexes, recognized as "life pigments", playing indispensable roles in life processes.[1–5] The functional prowess of porphyrins, encompassing biochemical, enzymatic, and photochemical functions, primarily hinges upon the unique attributes of their tetrapyrrole macrocycles.[6–8] Numerous porphyrins and their derivatives have been deliberately synthesized to serve diverse purposes, acting as catalysts, electron transport materials, DNA-binding or cleavage agents, photoluminescent molecules, and photosensitizers.[9,10] The conjugated macrocyclic structure of porphyrins furnishes a firm and stable coordination environment for central metals, rendering them compelling contenders for catalytic reactions involving various classes of metal-active centers.[11,12] Despite these merits, challenges arise due to potent π–π interactions between planar polyaromatic macrocycles, resulting in low solubility in aqueous solutions, susceptibility to agglomeration and deactivation, and a propensity to burst when employed as photosensitizers. These limitations significantly curtail their practical applications in biological contexts, such as biomimetic catalysis, biosensors, and drug delivery.[13,14] To surmount these hurdles, establishing specific covalent bond connections between distinct porphyrin molecules becomes pivotal. This strategy, coupled with catalytic synthesis of crystalline organic polymers featuring a porous structure, effectively addresses the drawbacks associated with free porphyrin molecules in practical applications. Additionally, the covalent bonds serve as conduits for electron transfer between different porphyrin monomers, thereby enhancing electron transfer efficiency and expanding the scope of their practical applications.

Covalent organic frameworks (COFs) represent a distinctive category of crystalline organic polymers distinguished by their porous structure, characterized by a well-defined periodic backbone and an orderly arrangement of extended pores.[15–19] The versatility of COFs, stemming from their tunable backbone and pore structure, offers abundant docking positions as reactive active sites for various biochemical reactions.[13,20] Additionally, their relatively large surface area facilitates effective reactant adsorption and product desorption, garner-

[a]*Research Center for Environmental Functional Materials, College of Environmental Science and Engineering, Tongji University, 1239 Siping Road, Shanghai, 200092, P. R. China. E-mail: jma@tongji.edu.cn*
[b]*School of Civil Engineering, Kashi University, Kashi 844000, China*
[c]*College of Oceanography and Ecological Science, Shanghai Ocean University, No 999, Huchenghuan Road, Shanghai, 201306, P. R. China*
[d]*Department of Chemical, Biomolecular, and Corrosion Engineering, The University of Akron, Akron, Ohio 44325, USA. E-mail: zhengj@uakron.edu*
†These authors contributed equally to this work.

ing significant attention in recent years. The integration of porphyrin molecules as building blocks into COFs emerges as a transformative approach to address the limitations associated with free porphyrin molecules in practical applications. The structural topology of COFs, particularly the square connected topology, plays a critical role in crafting their porous architecture. Porphyrin-based COFs, utilizing square planar geometry porphyrin molecules as connectors, offer enhanced design flexibility compared to COFs constructed with other units.[21] These COFs often form thermodynamically stable 2D layered structures, stacking porphyrins into ordered π-arrays, conducive to photoexcited carrier generation under visible light.[22] Their macrocyclic conjugated structure supports efficient charge separation and electron mobility, positioning porphyrin-based COFs as promising materials for photoelectrical applications like biological detection and photoelectric imaging.[23] Additionally, the versatility in modifying porphyrin substituents with various functional groups lends these COFs a broad spectrum of properties. This incorporation imparts COFs with enhanced biological properties, including photosensitivity,[24] enzyme catalytic activity,[25] and biomolecule recognition.[26] Consequently, these modified COFs hold immense promise across diverse applications such as biosensors, biomimetic catalysis, and biomedical applications. The preparation of porphyrin-based COFs predominantly involves specific catalytic reactions, such as Brønsted acid-driven and transition metal catalyst-driven processes, establishing covalent bonds between other linker units and ligands on the porphyrin ring.[19,27] The selection of distinct covalent linking units and catalysts becomes pivotal in tailoring the structural framework of COFs, leading to various structural types. Given the design flexibility and ease of functionalization in COF structures, utilizing linker units with diverse spatial configurations for condensation reactions with porphyrin molecules allows for the creation of COFs with varied spatial orientations. These are broadly categorized into two-dimensional (2D) and three-dimensional (3D) porphyrin-based COFs (Fig. 1). While substantial efforts have been directed towards constructing diverse COF frameworks and exploring their practical applications, limited attention has been given to summarizing the synthetic methods of COFs wherein porphyrin molecules serve as the primary building blocks. This review focuses on bridging this gap, delving into the synthesis of porphyrin-based COFs and elucidating their progress in research, particularly in the realm of biological applications.

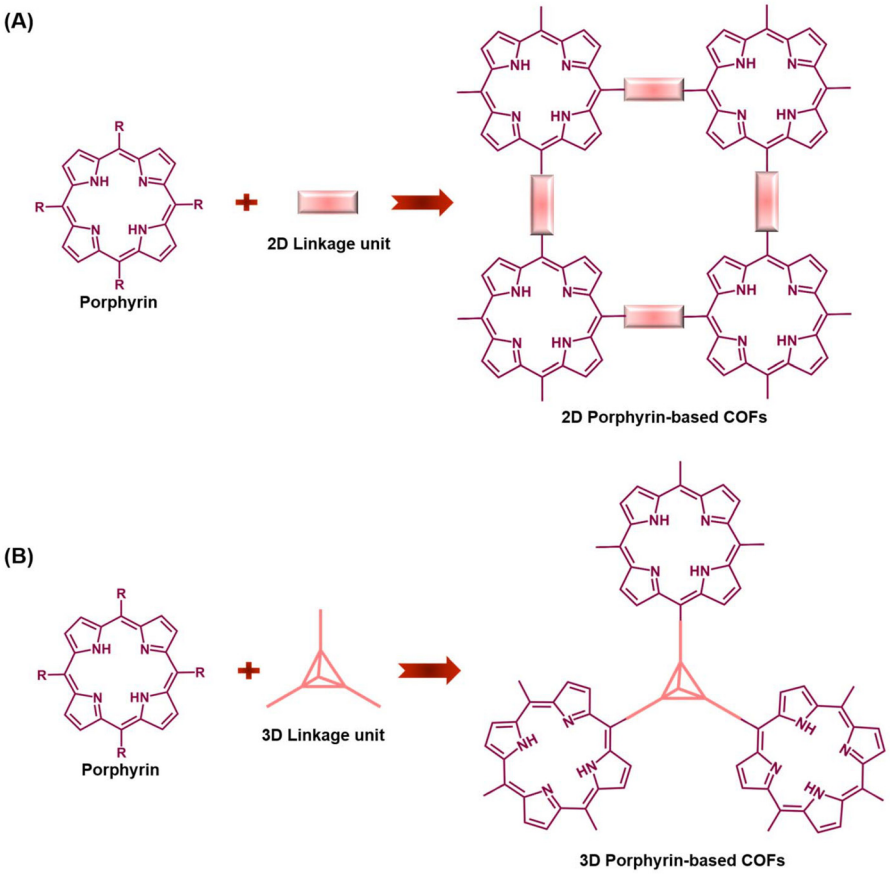

Fig. 1 Synthesis strategy for the assembly of porphyrin-based COFs: (A) 2D Porphyrin-based COFs; (B) 3D Porphyrin-based COFs.

2. Key challenges in the synthesis of porphyrin-based COFs

The synthesis of covalent organic frameworks (COFs) typically follows a common strategy, relying on dynamic covalent chemistry to achieve crystallinity through reversible bond formation. However, several key scientific issues need attention in the synthesis of porphyrin-based COFs. Firstly, the existing repertoire of reaction types for the synthesis of organic COFs is limited, especially considering the necessity for the reversibility of covalent bond formation. Consequently, the choice of building monomers with suitable reactivity becomes critical. In the case of porphyrin as a building unit, achieving reversible chemical bonding involves selecting porphyrin monomers with substituents at the meso position that exhibit compatible chemical activities in the reversible covalent bonding synthesis system. This prerequisite serves as a key factor in the successful preparation of porphyrin-based COFs. Furthermore, the structural modulation of the synthesized porphyrin-based COFs, encompassing aspects like layer spacing, crystallinity, porosity, and defects, plays a pivotal role in understanding the interrelationship between the material's structure and its properties. Addressing these key scientific challenges is essential to advancing the synthesis and understanding of porphyrin-based COFs for diverse applications.

2.1. Porphyrin monomers for porphyrin-based COFs

The critical role of substituents at various positions on porphyrin monomers greatly influences the formation of covalent bonds in porphyrin-based COFs, highlighting the importance of synthesizing appropriate porphyrin monomers. Modifications to the porphyrin core or the addition of different substituents imbue these monomers with a wide range of chemical and biological properties.[28] A key example is median porphyrin, known for its electron transfer capabilities and straightforward synthesis, making it a vital monomer in porphyrin research. Presently, median porphyrin is synthesized through several methods, including Rothemund's, Alder's (propionic acid method), Lindsey's, Macdonald's ([2 + 2] method), and microwave excitation methods. Among these, the Alder method, or propionic acid method, is frequently used. This method involves the condensation of aldehydes with varied substituents and pyrroles in an acidic medium, catalyzed by Lewis acid, resulting in porphyrin monomers with diverse substituents such as amino, aldehyde, hydroxyl, and others.

The synthesis methods employed for porphyrin-based covalent organic frameworks (COFs) closely parallel those used for other COF materials.[29,30] Thermodynamically controlled covalent chemistry (DCC) serves as the foundational principle for generating highly crystalline COF structures. This approach relies on the thermodynamic stability of COFs with ordered stacking, surpassing that of small-molecule zwitterions or amorphous polymers.[18,19,22] Consequently, DCC reactions are predisposed to yielding COFs with superior crystalline morphology, where covalent bonds undergo a dynamic process of breakage, transformation, and regeneration to reach a thermodynamically stable state.[31] In the synthesis of porphyrin-based COFs, covalent bond formation hinges on the functional groups within the porphyrin monomers and linkers. Fig. 2 illustrates the preparation of porphyrin derivatives (Por-1-8) featuring aldehyde, amino, fluorine, terminal alkyne, hydroxyl, and carboxyl groups. These derivatives react with specific catalytic linkers (Fig. 3), leading to a diverse array of covalent bonds. Throughout this process, continual identification and

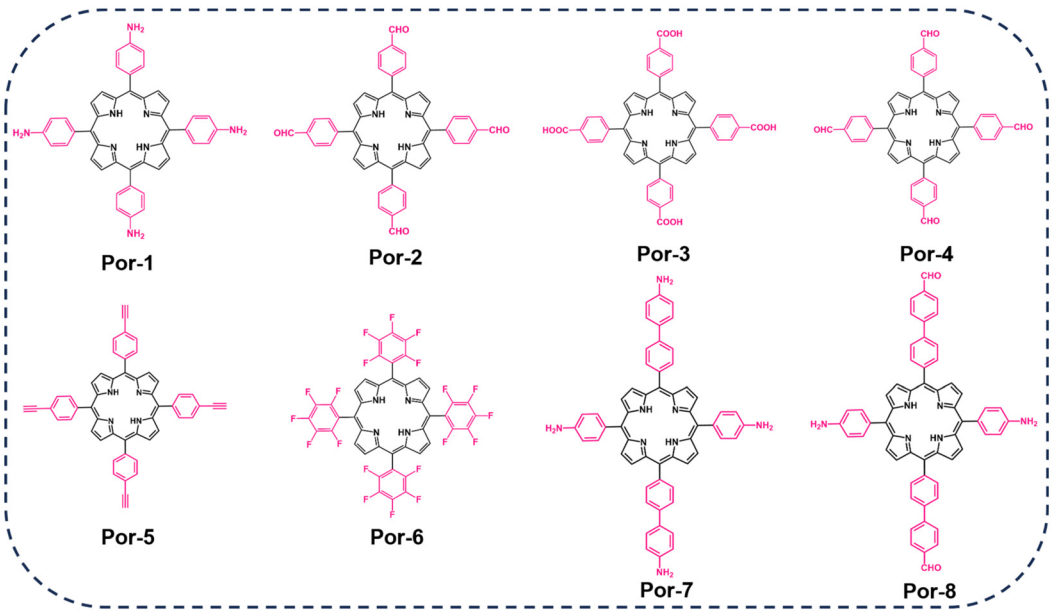

Fig. 2 Porphyrin monomers employed in the synthesis of porphyrin-based COFs.

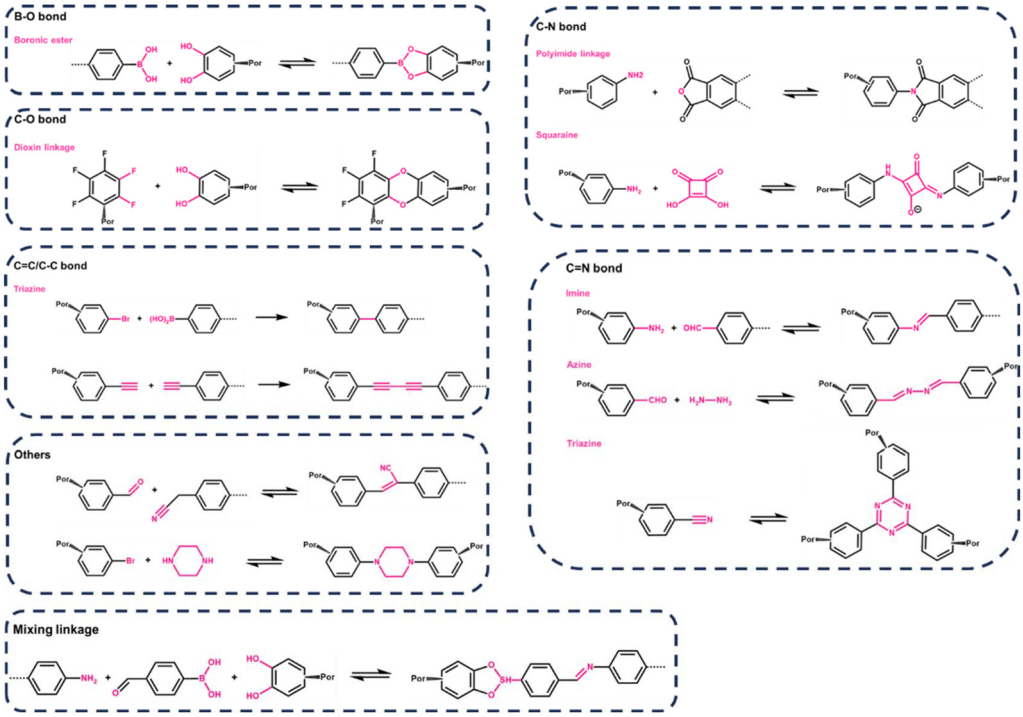

Fig. 3 Synthetic reaction routes employed in the fabrication of porphyrin-based COFs.

repair of structural defects occur—a continuous "self-diagnosis" and "self-repair" mechanism—resulting in an organic framework with a crystalline structure.[19,32] The rigidity and planarity of porphyrin molecules contribute to the superior controllability and crystallinity of COFs derived from porphyrin building blocks.[20,33] However, due to the intricate topology of porphyrin, a limited number of precursors are reported for synthesizing porphyrin-based COFs. Representative approaches include borate condensation, triazine condensation, and imide condensation.[34] Notably, innovative methods have emerged, such as the Yamamoto self-coupling reaction, cubic acid amine condensation, and one-pot esterification reaction, broadening the synthetic possibilities for COFs in recent years.[35]

2.2. Synthetic strategies for porphyrin-based COFs

Presently, the synthesis of porphyrin-based covalent organic frameworks (p-COFs) predominantly revolves around three symbiotic bond types: imine, borate, and triazine. Boronic acid and catechol-based monomers undergo reversible transformations, resulting in the formation of a borate five-membered ring structure. Self-condensation of boronic acid leads to planar linkages of boron oxo-six-membered rings. Generally, porphyrin COFs containing boron exhibit commendable thermal stability, high crystallinity, and a substantial BET surface area, albeit displaying vulnerability under aqueous acidic conditions. In contrast, p-COFs linked by amino condensation to generate imine bonds demonstrate enhanced chemical stability in aqueous, acidic, and alcoholic complex systems but with a trade-off of relatively lower crystallinity. In response to this, researchers have explored a hybrid approach, combining boronic acid and imine bonds to create multifunctional covalent bonding linkages. This endeavor aims to achieve a delicate balance, allowing the COFs to simultaneously exhibit high crystallinity and exceptional stability. Notably, Jiang *et al.* proposed a two-stage approach for synthesizing porphyrin-like functionalized COFs incorporating imine and boronic acid bonds.[36] This strategy increased the structural complexity by introducing bifunctional linkages, enriching the repertoire of structural units.

However, recent studies have broadened the understanding of diverse covalent bonding in COF designs, leading to an expanded focus on varied connections. An exemplary case is squaric acid, a dye known for its versatile applications including imaging and photodynamic therapy, characterized by its amphiphilic ion resonance structure. The condensation of squaric acid with *p*-toluenesulfonic acid creates squaraine (SQ) with a distinctive planar zigzag structure. Building on this, Nagai *et al.*[37] employed 5,10,15,20-tetrakis (4-aminophenyl) porphyrin copper (TAP-CUP) as a foundational component to synthesize a two-dimensional conjugated COF, CUP-SQ COF, featuring a tetragonal mesoporous structure. This COF's zigzag conformation enhances structural stability, solvent resistance, lowers band gap energies, and significantly increases absorptivity, setting it apart from conventional COFs. Furthermore, while the synthesis of borate- and imine-conjugated COFs often necessitates harsh conditions such as elevated temperatures, pressures, inert atmospheres, non-homogeneous mix-

tures, and extended durations. Nath *et al.*[38] presented a milder approach. They achieved the synthesis of azodioxo (–on-π, NO–) bond-conjugated porphyrin two-dimensional COFs with enhanced optoelectronic properties through a homogeneous solution reaction at room temperature, demonstrating the feasibility of fabricating P-COFs under considerably gentler reaction conditions. In recent advancements, enhancing the stability of P-COFs has captivated the interest of numerous researchers. It's theorized that 2D sp^2 carbon chain-connected P-COFs, with their fully conjugated carbon atoms, possess high chemical stability and exhibit minimal reversibility in their synthesis process. Chen *et al.*[39] developed a two-dimensional (2D) porphyrin-based sp^2 carbon-conjugated COF (Por-sp^2c-COF). When employed in photocatalysis, the sp^2 carbon-conjugated backbone of these COFs enables p-conjugation in both *x* and *y* directions. This arrangement potentially allows for more efficient transport of p-conjugation throughout the 2D lattice, thereby enhancing electron delocalization.

The summarized types of covalent bond-forming reactions commonly employed for synthesizing porphyrin COFs are depicted in Fig. 3. This exploration of diverse synthetic strategies enhances our understanding of p-COFs, offering avenues to tailor their properties for specific applications.

2.3. Control of crystallinity, pore structure, and defects for Porphyrin-based COFs

Enhancing the crystallinity, porosity, and stability of covalent organic framework (COF) materials is imperative for their development. Achieving improved intra- and interlayer interactions is now feasible through supramolecular interactions. For instance, incorporating complementary π interactions at the edges between layers significantly boosts interlayer forces, leading to enhanced crystallinity, porosity, and stability (Fig. 4A).[40] Introducing intra-layer hydrogen bonding interactions into the edge units has also proven effective in enhancing the crystallinity, porosity, and π-conjugation of imine-connected COFs (Fig. 4B).[41,42] The pores of conventional COFs typically exhibit well-defined polygonal shapes, ranging from hexagonal and quadrilateral to triangular and rhombic structures, with sizes varying from small micropores to large mesopores. In the case of porphyrin-based COFs, the regular planar structure of porphyrin imparts a predominantly regular tetragonal structure to the pores. The pore size can be finely regulated by adjusting the lengths of different substituents or linkers in the porphyrin structure. Noteworthy examples include the green synthesis of multifunctional COFs by Zhang *et al.*,[43] utilizing porphyrin and phthalocyanine as building blocks with water as the solvent. The directional regulation of COF pore structure was achieved by modifying the porphyrin or phthalocyanine ligands. Similarly, Yue *et al.*[44] reported on COFs with phthalocyanine molecules linked by dioxin bonds, showcasing the micro-regulation of pore size from 1.3 nm to 1.1 nm through the selection of different monomers.

In the course of COF synthesis, the inevitability of defects arises due to the incomplete reaction of all functional groups. These defects encompass issues arising not only during the synthesis and handling of COFs but also include undercrystallization, stacking disorder, and network vacancies. In specific chemical reactions, the reactivity of COFs is influenced by these defects, thereby modifying the materials properties, including electronic structure, wettability, periodic pore size, and affinity for identified chemicals. Consequently, the challenge lies in minimizing defects and harnessing their potential for new properties and applications, a topic garnering significant attention. Research by Daliran *et al.*[45] addresses defect minimization by advocating for a strategic mix of building blocks. Their findings revealed that during polymerization, design components with one or two reactive groups undergo linear growth from their ends (Fig. 4C). In contrast, monomers capable of constructing hexagonal networks exhibit uniform growth in all directions, suggesting that hexagonal building blocks are an optimal choice for significantly reducing defects in rings formed by monomer, dimer, and trimer building blocks. An alternative strategy for defect control involves reticulation chemistry through the geometric selection of building blocks, akin to a monomer symmetry modulation approach. The interplay between building blocks can influence the reversible transition between ordered and disordered states, shaping the resulting material. Kandambeth *et al.*[42] proposed a notably resilient imino-based porphyrin COF that establishes intranetwork hydrogen bonds. By utilizing dihydroxyterephthalaldehyde as a ligand, they established connections to the imine N (Fig. 4D) *via* hydrogen bonding. The research demonstrated a robust non-covalent conformational locking effect, revealing that higher hydrogen bonding interactions led to lower defects, as evidenced by pore distribution and texture characterization.

3. Biological applications of porphyrin-based COFs

3.1. Biocatalytic applications

Living organisms often harbor metal porphyrins, such as magnesium porphyrin in chlorophyll and iron porphyrin in the active center of hemoglobin. This has spurred significant interest in biomimetic catalysis based on metal porphyrin derivatives, engaging in various processes. Leveraging superior biomimetic activity and catalytic stability, porphyrin-based covalent organic frameworks (COFs) have exhibited exceptional performance in diverse catalytic reactions, including CO_2 reduction, photocatalytic hydrogen and oxygen generation, and chemical synthesis. Addressing the challenge of electrochemically reducing carbon dioxide (CO_2) to valuable hydrocarbons and chemical feedstocks (alcohols, aldehydes, ketones, *etc.*) represents a promising technological approach to mitigate CO_2 emissions and address energy challenges.[35,46–48] However, common issues in electrochemical CO2 reduction, such as low reaction rates and poor selective production rates of intermediates, persist. The advantages of porphyrin-based COF catalysts in electrochemical CO_2 reduction processes lie in their ability to facilitate gas mass

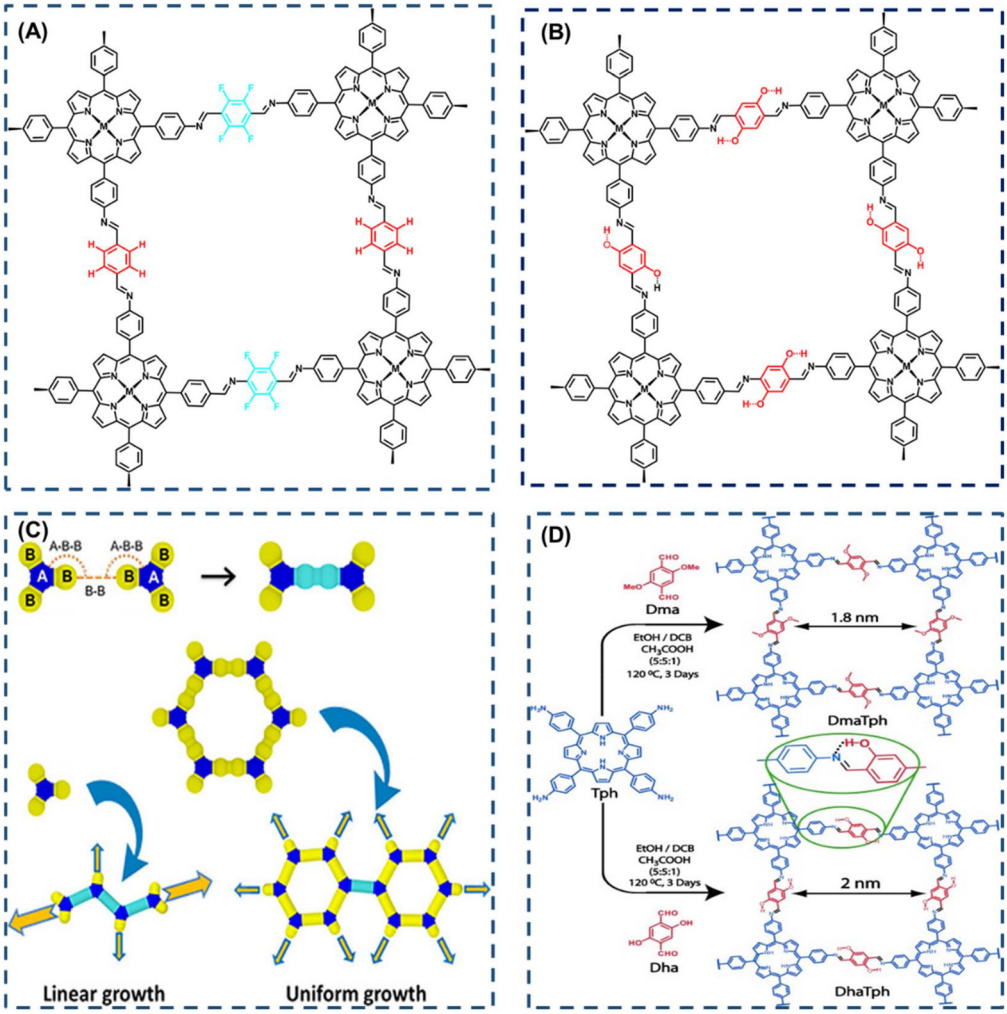

Fig. 4 (A) Interlayer complementary π interactions in CuP-TFPh 50% COF. Reproduced with permission of Ref. 40. Copyright © 2012, Xiong, American Chemical Society. (B) Intralayer hydrogen-bonding interaction in COF (M = H_2), also known as MP DHPh COF (M = H_2, Cu, or Ni). Reproduced with permission of Ref. 41. Copyright © 2015, Chen, American Chemical Society. (C) Computational studies on (a) polymerization model according to the topology of the monomer. Reproduced with permission of Ref. 42. Copyright © 2021, Daliran, Wiley. (D) Interactions between building blocks: intraframework hydrogen bonding. Reproduced with permission of Ref. 45. Copyright © 2013, Kandambeth, Wiley.

transfer and adsorption.[49–52] These catalysts offer high specific surface area, tunable porosity, and a regularly ordered structure. These characteristics position porphyrin-based COFs as effective choices for electrochemical CO_2 reduction, contributing to the advancement of sustainable and efficient methods for minimizing carbon emissions.[53–55]

Gong *et al.*[56] employed the porphyrin-based covalent organic framework TPPDA-CoPor-COF, synthesized through cross-condensation of 5,10,15,20-tetrakis(4-benzaldehyde) porphyrin with tetraphenyl p-phenylenediamine (PPDA). This COF exhibited an impressive 87–90% CO Faraday efficiency within the range of −0.6 to −0.9 V relative to RHE (Fig. 5A). The electronic properties of porphyrins can be fine-tuned by altering substituents at various sites (meso/beta-sites) on the porphyrin macrocycle, thereby influencing the practical performance of these molecules. The positional and structural differences of substituents on the porphyrin ring contribute to the diverse properties of the porphyrin molecules. In a recent study, Ren *et al.*[57] designed a nitrogen-miscible metalloporphyrin covalent organic frameworks through the condensation of 5,10,15,20-tetrakis(4-benzaldehyde) porphyrin with p-phenylenediamine (PPDA). Notably, altering the central metal coordination structure of the porphyrin molecule through nitrogen elemental doping increased the electron density on the cobalt (Co) atom at the center of the metalloporphyrin (Fig. 5B). This adjustment elevated the d-band center, providing stabilization to the crucial intermediate in the potential-determining step of the electroreduction of CO_2. Consequently, this modification facilitated the profound reduction of CO_2 to form carbon C1 products such as CH_3OH and CH_4, concurrently improving the selectivity of the reaction products.

Metal-N_4 coordination structures loaded onto carbon or porous polymers are recognized as highly effective catalytic sites for CO_2 reduction reactions (CO_2RR).[58–61] The well-

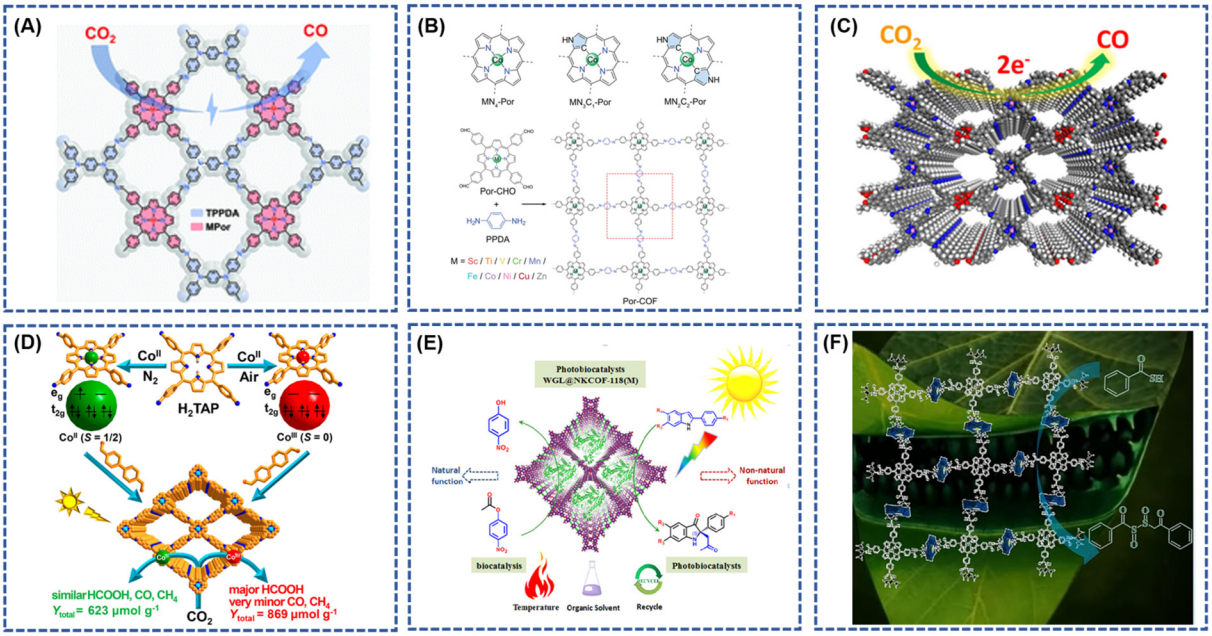

Fig. 5 (A) The schematic diagram of the electrochemical reduction of CO_2 by TPPDA-CoPor-COF; reproduced with permission of Ref. 56. Copyright © 2022, Gong, the Royal Society of Chemistry. (B) Structural scheme of MN_4-Por, MN_3C1-Por, MN_2C_2-Por, and Por-COFs condensed by M-[5,10,15,20-tetrakis(4-benzaldehyde) porphyrin] (Por-CHO) and p-Phenylenediamine (PPDA); reproduced with permission of Ref. 57. Copyright © 2023, Ren, Wiley. (C) The schematic diagram of the electrochemical reduction of CO_2 by crown ether and cobalt-porphyrin-based COF (TAPP(Co)-B18C6-COF); reproduced with permission of Ref. 65. Copyright © 2021, An, American Chemical Society. (D) Rational Fabrication of COF-367-Co Featuring Different Spin States of Co Ions toward Photocatalytic CO_2 Reduction; reproduced with permission of Ref. 66. Copyright © 2020, Gong, American Chemical Society. (E) Schematic representation of the WGL@COFs photobiocatalyst for enantioselective Mannich reaction under visible light irradiation; reproduced with permission of Ref. 68. Copyright © 2022, Jin, American Chemical Society. (F) Schematic diagram of catalytic conversion desulfurization over the MnTP@ZnAdCOF catalysts. Reproduced with permission of Ref. 69. Copyright © 2023, Mushtaq, Elsevier.

defined structures of porphyrin-based covalent organic frameworks (COFs) facilitate the formation of Metal-N_4 complexes, enabling precise tuning of CO_2RR performance.[62,63] Despite their advantageous structures, the inherent strong hydrophobicity and limited electron transfer ability of COFs constrain their catalytic efficiency.[64] Addressing these limitations, An *et al.*[65] developed a crown ether and cobalt porphyrin-based COF (TAPP(Co)-$B_{18}C_6$-COF) for CO_2 reduction catalysis. The introduction of the crown ether unit not only enhanced the hydrophilicity of the framework but also facilitated electron transfer from the crown ether to the coproporphyrin nucleus. Additionally, the crown ether unit augmented the CO_2 binding capacity (Fig. 5C). Consequently, these modified COFs demonstrated outstanding catalytic performance, achieving Faraday efficiencies (FECO) between 84.4% and 93.2% at applied potentials ranging from −0.60 to −0.90 V *vs.* RHE, with a maximum turnover frequency (TOF) of 1267 h^{-1} at −0.9 V. In a separate study, Gong *et al.*[66] obtained Co^{II}-TAP by reacting porphyrin tetraphenylamine (H_2TAP) with $Co(CH_3COO)_2 \cdot 4H_2O$, followed by spontaneous oxidation in air to yield CoIII-TAP. The corresponding COFs (COF-367-Co^{II} and COF-367-Co^{III}) were synthesized through solvothermal methods involving Co^{II}-TAP/Co^{III}-TAP and BPDA reactions (Fig. 5D). Theoretical calculations, supported by multiple experimental verifications, revealed that the spin ground states of Co^{II} and Co^{III} in COF-367-Co^{II}/COF-367-Co^{III} are S = 1/2 and S = 0, respectively. Photocatalytic CO2 reduction results indicated that the Co^{III} site in COF-367-Co^{III} favors the formation of HCOOH, while hindering the further conversion of HCOOH to CO and CH_4. Consequently, COF-367-Co^{III} exhibited higher photocatalytic activity and selectivity for HCOOH production compared to COF-367-Co^{II}.

Porphyrin-based COFs showcase captivating properties, particularly in photoelectrochemical conversion efficiencies within catalytic reactions featuring metal porphyrin molecules. Notably, active centers like magnesium porphyrin or iron porphyrin exhibit biomimetic catalytic activity and enzymatic reactivity. Zhu *et al.*[67] demonstrated the utility of two porphyrin COFs as efficient heterogeneous photocatalysts for photoinduced electron transfer reversible addition–fragmentation chain transfer (PET-RAFT). Leveraging porphyrins with robust donor–acceptor characteristics and off-domain conduction bands, these COFs facilitated visible-light-driven polymerization of a wide range of monomers in both organic and aqueous mediums. The resulting polymers exhibited adjustable molecular weights (MW), low molecular weight dispersions, and exceptional chain end integrity through at least five iterations of PET-RAFT polymerization.

Challenges persist in merging photocatalysis and biocatalysis for the creation of photobiocatalysts tailored for asymmetric catalysis. Jin *et al.*[68] successfully immobilized wheat

germ lipase (WGL) onto a mesoporous solid carrier composed of meticulously designed photocatalytic porphyrin covalent organic frameworks (COFs). This innovative photo-enzymatic platform demonstrated robust operational stability, high enzyme activity, and effective enantioselective Mannich processes under visible light irradiation (Fig. 5E). The co-localization of the photocatalyst and enzyme within a single arrangement contributed to the satisfactory efficiency and reusability of the WGL@COFs photobiocatalysts. In a separate endeavor, Afshan Mushtaq *et al.*[69] synthesized a novel covalent organic framework, MnTP@ZnAdCOF, under mild reaction conditions using H_2O_2 as the oxidant. This framework served as a heterogeneous catalyst in the presence of H_2O_2, producing reactive intermediates [(Por)(OAc)Mn-OOH]-, [(Por)(OAc)MnIVdouble bondO], and Mo(O_2). Notably, the MnTP@ZnAdCOF catalyst exhibited a desulfurization efficiency of up to 98%, catalyzing the conversion of dibenzothiophene, thiobenzoic acid, and various sulfur-containing compounds to sulfoxide at 25 °C (Fig. 5F). This method showcased remarkable efficacy in oxidizing sulfur-containing compounds in diesel, contributing to a reduction in fuel sulfur content.

3.2. Biosensors

The porphyrin molecule, renowned for its outstanding photosensitivity and stability, proves adept at discerning minute changes in photoelectric signals through electrochemical processes or various spectroscopic methods, including UV, IR, fluorescence, phosphorescence, and Raman.[3,25,67,70–72] This unique capability facilitates the detection of target molecules and enables analytical conclusions, presenting compelling opportunities for applications in the realm of photoelectrochemical biosensors.[73,74] However, biosensors employing pure porphyrin molecules as the photoelectrical reaction entity encounter limitations in luminescence efficiency.[75] The unique properties of 2D layered nanostructures, including reduced charge transfer times and distances along with distinctive optical and electrical characteristics, make them ideal for photoelectrochemical biosensing. Porphyrin-based covalent organic frameworks (P-COFs), which incorporate natural porphyrin molecules as building units, introduce enhanced biological functionalities to these 2D materials for biological detection.[76] For instance, Cui *et al.* developed an aptamer-based electrochemical sensor to detect *Escherichia coli*. This sensor employs a porphyrin-based covalent organic framework (TPH-TDC-COF), constructed from 5,10,15,20-tetrakis(4-aminophenyl)-21*H*,23*H*-porphyrin (TPH) and [2,2′-bithienyl]-2,5′-dicarboxaldehyde (TDC). The TPH-TDC-COF's highly conjugated structure, along with its favorable electrical conductivity, large surface area, and enhanced biocompatibility, significantly improves its ability to anchor *E. coli*-targeting aptamers. In optimal conditions, this electrochemical aptasensor achieved a detection limit of 0.17 CFU mL^{-1} for *E. coli*, within a linear range of 10 to 1×10^8 CFU mL^{-1} (ref. 77). Recent research suggests that introducing co-reactants into the electrochemiluminescence (ECL) system can significantly enhance porphyrin's luminescence efficiency. Wang *et al.*[78] synthesized a composite probe (Zn-TCPP-TiO_2-$Ti3C_2$) by uniting luminophores (Zn-TCPP) with co-reactants (TiO_2 nanoparticles) using a solvothermal method. This composite was structured with tripropylamine-modified gold nanoparticles (TPrA@AuNPs) anchored onto Zn-TCPP-TiO_2-Ti_3C_2 to form a sandwich configuration. When activated electrically, electrons move from TiO_2 valence band, generating holes (h^+). These holes, when injected into the tripropylamine (TPrA) molecule lowest unoccupied molecular orbital (LUMO), generate extra $TPrA^+$ ions, enhancing the electrochemiluminescence (ECL) signal. The strategic placement of TiO_2 as a co-reactant not only concentrates co-reactants at the electrode interface but also significantly reduces the distance for electron transfer to the luminophore and co-reactant, boosting the ECL signal. The inclusion of TiO_2 in the TPrA@AuNPs/Zn-TCPP system resulted in a 3.5-fold signal increase compared to the system without TiO_2. The formation of covalent bonds in porphyrin-based covalent organic frameworks (COFs) enhances the transfer of photogenerated electrons, positioning them as promising materials for photosensitive components in photoelectrochemical (PEC) sensors. The efficient conversion of photoelectric signals is pivotal for assessing the performance of sensors in photoelectrochemical applications. Current research emphasizes the broad spectrum of applications, including the detection of pH,[24] proteins,[79] DNA,[80] ions,[14] and gases,[7] showcasing the versatility and potential of porphyrin-based COFs in advancing biosensor technologies.

Simultaneously, within the electrochemiluminescence (ECL) system, the synthesized covalent organic frameworks (COFs) featuring metalloporphyrin as the constructs, with abundant open metal sites, enable precise regulation of ECL performance. This fine-tuning enhances the formation of reaction intermediates and collision efficiency during the ECL reaction process, thereby further elevating the luminescence efficiency of metalloporphyrin COF biosensors.[81,82] In a study by Zhang *et al.*,[83] a two-dimensional (2D) porphyrin covalent organic framework (p-COF) was proposed as the foundation for a photoelectrochemical (PEC) sensitive sensor designed for label-free detection of C-reactive protein (CRP). The resulting p-COF exhibited heightened conductivity and enhanced stability due to the formation of covalent bonds characterized by exceptional stability (Fig. 6A). The introduction of p-COF hindered the complexation of electrons and holes, narrowing their band gap (E_g), consequently improving photocurrent conversion efficiency. In comparison to pure porphyrins, p-COFs demonstrated increased photocurrent intensity. Furthermore, Zheng *et al.*[84] developed a colorimetric-photoelectrochemical dual-mode biosensor for *S. aureus* based on FePor-TPA. Through the *in situ* growth of a 2D FePor-TPA film on an ITO electrode, a more ordered stacking pattern with well-defined conductivity, stable initial photocurrent, and high sensitivity to O_2 was achieved (Fig. 6B). The dual-mode photoreaction signal of the iron boride, originating from two independent modes, not only provides verification but also calibration, significantly enhancing the sensitivity and selectivity of *Staphylococcus aureus* detection.

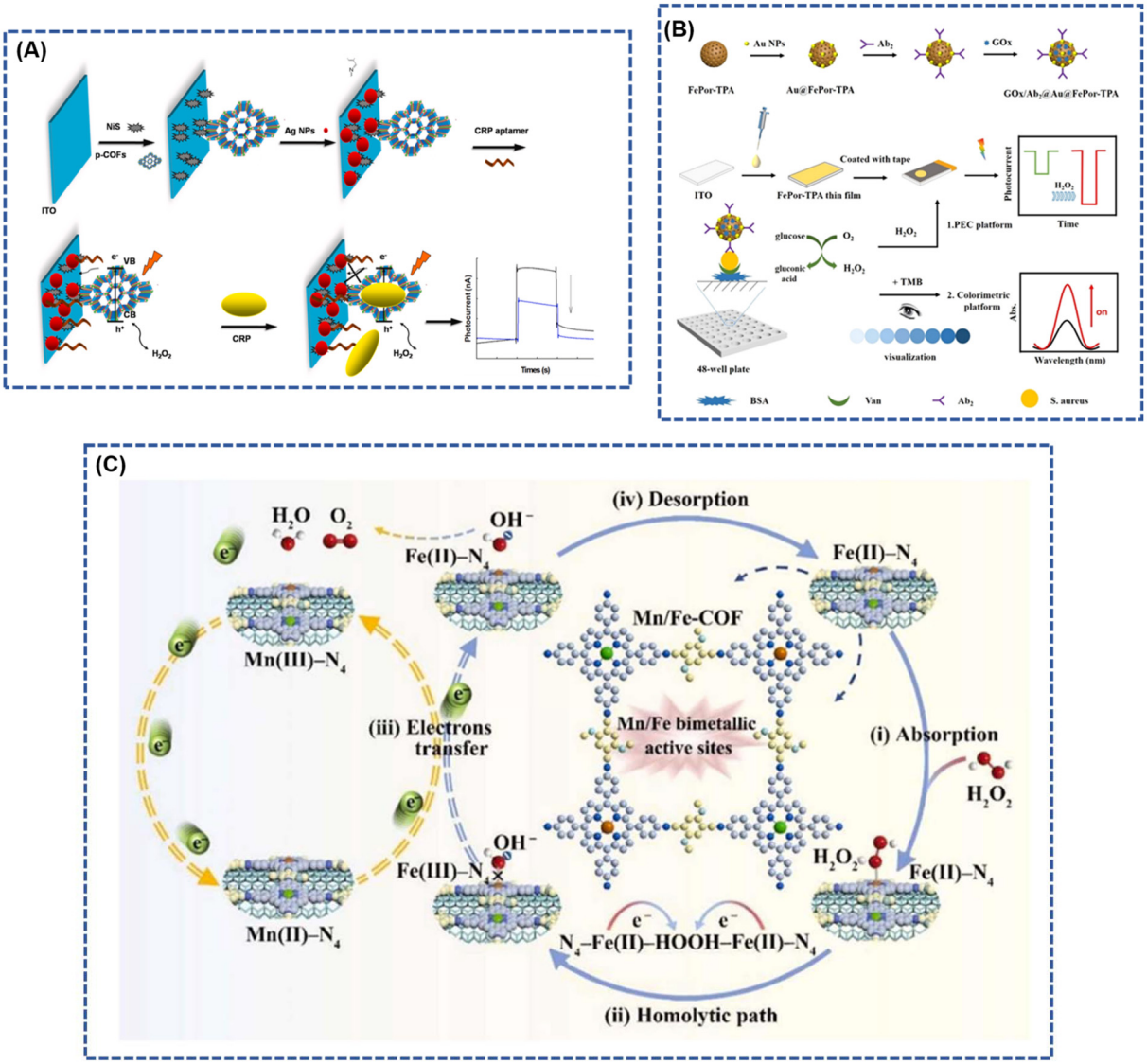

Fig. 6 (A) Stepwise fabrication procedure of CRP photoelectrochemical biosensors; reproduced with permission of Ref. 83. Copyright © 2019, Zhang, Elsevier. (B) Principle of the constructed dual-mode immunosensor for *S. aureus* detection; reproduced with permission of Ref. 84. Copyright © 2023, Zheng, American Chemical Society. (C) Mechanism of electrocatalytic oxidation of H_2O_2 by MWCNTs@Mn/Fe-COF modified electrode. Reproduced with permission of Ref. 61. Copyright © 2023, Bai, Elsevier.

The p-COF biosensor is meticulously crafted by selecting a metal porphyrin characterized by a well-defined M–N_4 coordination structure. In this design, the metal ions at the center of the porphyrin ligand serve as electron transfer agents, enhancing the sensitivity of specific redox catalysis for the analyte.[85] This unique feature enables the simultaneous detection of multiple analytes in complex environments.[58,61] Bai *et al.*[61] introduced a covalent organic framework biomimetic electrochemical sensor (MWCNTs@Mn/Fe-COF) based on bimetallic porphyrins. The sensor involves the *in situ* polymerization of manganese porphyrin (MnPor) and iron porphyrin (FePor) on multi-walled carbon nanotubes (MWCNTs) for the precise determination of trace H_2O_2 (Fig. 6C). The distinctive topological attributes of the COF, coupled with the exceptional electrical conductivity of MWCNTs as highly independent M–N_4 electrochemical active sites, create a robust electron transfer pathway. Notably, the introduction of manganese (M_n) sites instigates a self-accelerating redox cycle between valence states, significantly amplifying electrocatalytic efficiency. This innovative approach achieves ultrasensitive detection of H_2O_2, demonstrating a remarkable detection limit as low as 2 nM.

Cui *et al.*[79] innovatively designed a fluorescent sensor utilizing a porphyrin covalent organic framework (p-COF) and carbon dots (CDs) for the detection of vascular endothelial growth factor 165 ($VEGF_{165}$) and imaging the breast cancer cell line Michigan Cancer Foundation-7 (MCF-7). This sensor demonstrated an impressive detection limit for $VEGF_{165}$, reaching 20.9 fg mL^{-1} within a broad linear range spanning 1.0 pg mL^{-1} to 100 ng mL^{-1}

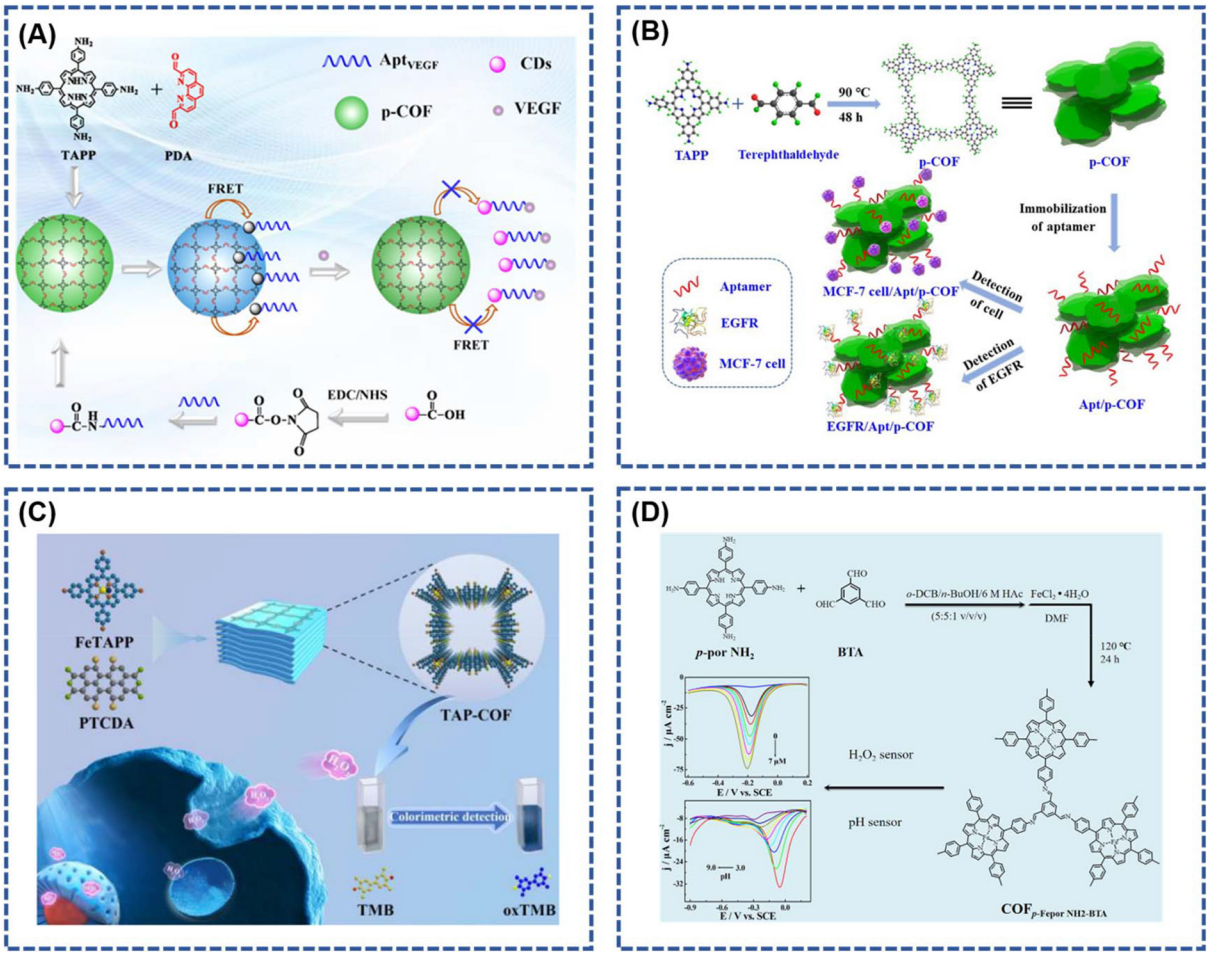

Fig. 7 (A) Schematic representation of the p-COF-based fluorescence biosensor; reproduced with permission of Ref. 79. Copyright © 2023, Cui, American Chemical Society. (B) Schematic diagram of the p-COF-based aptasensor for detecting EGFR or MCF-7 cells; reproduced with permission of Ref. 86. Copyright © 2019, Yan, Elsevier. (C) Diagrammatic drawing for the synthesis of TAP-COF and *in situ* detection of H_2O_2 released from MCF-7 cells; reproduced with permission of Ref. 20. Copyright © 2023, Wang, Elsevier. (D) Schematic representation of the $COF_{p\text{-Fepor NH}_2\text{-BTA}}$ sensor applied as a simulated peroxidase for H_2O_2 detection. Reproduced with permission of Ref. 24. Copyright © 2020, Xie, Elsevier.

(Fig. 7A). Moreover, the developed fluorescent biosensor was effectively applied to detect VEGF165 expression in MCF-7 cancer cells. In a separate study, Yan *et al.*[86] synthesized a porphyrin-based covalent organic framework (p-COF) through a straightforward oil bath method and employed it as a novel sensing layer for immobilizing epidermal growth factor receptor (EGFR)-targeted drugs (Fig. 7B). The resulting sensitive sensor, based on the p-COF, exhibited an exceptionally low detection limit (LOD) of 5.64 fg mL^{-1} using differential pulse voltammetry and 7.54 fg mL^{-1} using electrochemical impedance spectroscopy. This sensor demonstrated a broad linear detection range spanning 0.05–100 pg mL^{-1} of EGFR concentration, showcasing its potential for highly sensitive and versatile applications.

Wang *et al.*[20] conducted the preparation of a porphyrin-based porous covalent organic framework (TAP-COF) through a one-step condensation process involving 1,6,7,12-tetrachloroethylenetetracarboxylic dianhydride and 5,10,15,20-tetra(4-aminophenyl)porphyrin iron(III) (Fig. 7C). The resulting TAP-COF exhibits notable characteristics, including a high specific surface area, abundant surface catalytic active sites, and an exceptionally efficient electron transport capacity. This is attributed to its precisely controlled donor–acceptor arrangement and a three-dimensional porous structure. The TAP-COF demonstrates outstanding peroxidase catalytic activity, effectively catalyzing the oxidation of the substrate 3,3′,5,5′-tetramethylbenzidine by H_2O_2, resulting in a distinctive blue reaction. Similarly, Xie *et al.*[24] reported the application of an iron porphyrin-based covalent organic framework ($COF_{p\text{-Fepor NH}_2\text{-BTA}}$) for electrochemical sensing of H_2O_2 and pH. The synthesis of the porphyrin-based COF ($COF_{p\text{-por NH}_2\text{-BTA}}$) involved an aldol-ammonia condensation reaction between 1,3,5-benzotrialdehyde and 5,10,15,20-tetrakis(4-aminophenyl)-21*H*,23*H*-porphine. The COFp-Fepor sensor displayed commendable H_2O_2 detection capability within the range of 6.85 nM to 7 μM, featuring a detection limit of 2.06 nM (S/N = 3), and exhibited pH detection in the range of 3.0 to 9.0 (Fig. 7D). Table 1 summarized the key parameters of the above porphyrin-based COFs for biosensor applications.

Table 1 Key parameters for sensing performance assessment of different p-COFs sensors

Materials	Detection targets	Detection limits	Selectivities	Ref.
TAP-COF	H_2O_2	2.6 nM	Al^{3+}, Ca^{2+}, Mg^{2+}, Zn^{2+}, K^+, *etc.*	20
$COF_{p\text{-}Fepor\text{-}NH_2\text{-}BTA}$	H_2O_2/pH	2.06 nM	Glucose, fructose, mannose, DA, AA, *etc.*	21
MWCNTs@Mn/Fe-COF	H_2O_2	2 nM	Commercial disinfector, apple juice	58
Tph-TDC-COF	Escherichia coil	0.17 CFU mL^{-1}	Saa, Sta, Bas, Sty	73
Fe-COF-H3	UA	5 μmol L^{-1}	AA, Cly, Gly, NaCl, KCl, urea, BSA	74
$Apt_{VEGF/CD}$	$VEGF_{165}$	20.9 fg mL^{-1}	BSA, HER2, PSA, PTK7, MUC1, CEA, AFP	75
2D P-COFs	CRP	0.1 ng mL^{-1}	PBS, PSA, BSA, HCG, gluccose	79
Apt/P-COFs	EGFR/MCF-7	5.64 fg mL^{-1}, 7.54 fg mL^{-1}	PBS, PSA, MUC1, HER2, VEGF, IgG, *etc.*	81

3.3. Cancer therapy

The realization of early diagnosis of cancer represents the key to the improvement of cancer treatment technology. The development of early cancer diagnosis technology is of great significance to improve the survival rate of patients.[87] The COFs with high porosity can realize favorable interaction with the guest molecules, which greatly improves the lower limit of detection of cancer cells and the performance of detection, and therefore can enhance the diagnosis of cancer early diagnosis rate. Due to the excellent optoelectronic properties of porphyrin molecules in their structures, the porphyrin-based COFs have gained wide attention in the research of optoelectronic imaging of tumor cells. Gao *et al.*[88] prepared a probe for cellular imaging by physically adsorbing dye-labeled nucleic acid recognition sequences onto carbonized COF nanoparticles (termed C-COF), which could efficiently illuminate biomarkers (Survivin and TK1mRNA) in living cells. The C-COF possessed an enhanced photothermal conversion capability, suggesting that the probe is also a photothermal therapy of the promising candidate for photothermal therapy. The carbonization eliminated the potential toxicity problem of the aromatic rigid building blocks of COFS, and developed biocompatible and multifunctional COF-derived nanoprobes for biomedical applications.

Photodynamic therapy (PDT) stands out as a promising anticancer strategy, harnessing photosensitizers to respond to light irradiation and generate lethal reactive oxygen species (ROS), particularly $^1O_2$, capable of disrupting the structural integrity of cancer cells.[13,14] In this context, the efficacy of photosensitizers in manufacturing ROS or achieving high photothermal conversion efficiency is crucial for successful phototherapy. Porphyrin-based covalent organic frameworks (COFs) exhibit advantageous characteristics, including consistent porosity, robust structural stability, and exceptional photosensitivity. The intrinsic stability of porphyrins and their derivatives ensures the reliable transport of ROS during treatment, overcoming the issues of decomposition and aggregation faced by traditional photosensitizers like chlorin 6 and indocyanine green under laser irradiation, thereby enhancing their photothermal conversion efficiency.

Porphyrins, recognized for their longest absorption spectrum in the red part, enable light penetration into deeper tissues, making them particularly useful for treating deep-seated tumors. Zhang *et al.*[26] innovatively designed COF-618-Cu, a porphyrin-based cross-stacked COF with outstanding catalase-like activity, serving as a reactive oxygen species (ROS) amplifier. COF-618-Cu effectively mitigates tumor hypoxia by utilizing endogenous hydrogen peroxide to produce ample oxygen (Fig. 8A). This addresses the inherent issues of photobleaching and aggregation-induced quenching (ACQ) associated with traditional photosensitizers, as well as the intrinsic antioxidant properties of the tumor microenvironment (TME). The synergistic effect of phototherapy and cancer immunotherapy is significantly improved by COF-618-Cu. In a TME-simulating environment (100 μM H_2O_2 and pH = 6.0), COF-618-Cu exhibits high oxygen production efficiency and desirable glutathione peroxidase (GPx) activity, simultaneously decomposing glutathione (GSH) to reduce ROS clearance. Employing a single light source with a 660 nm wavelength for irradiation achieves excellent results in both PDT and photothermal therapy (PTT), eliminating the need for secondary laser irradiation and saving treatment time. Wan *et al.*[89] synthesized 4,4′,4″,4‴-(porphyrin-5,10,15,20-tetrakis-yl)tetraphenylamine (TAPP) and 4,4′-(benzothiadiazole-4,7-diyl)dibenzaldehyde (BDA) as carbon-based nano-enzymes derived from COFs linked by imine bonds. These nano-enzymes enable synergistic catalytic therapy and second near-infrared (NIR-II) photothermal therapy for cancer (Fig. 8B). The developed nanozymes exhibit diverse enzyme-like activities, including oxidase (OXD)-like, catalase (CAT)-like, and peroxidase (POD)-like catalytic activities, generating ample anticancer reactive oxygen species (ROS) for effective cell killing.

Moreover, sonodynamic therapy (SDT) capitalizes on the deep tissue penetration capability of ultrasound (US) into biological tissues to focus acoustic energy, activating sonosensitizers for anti-tumor effects. This alternative strategy offers reduced trauma and damage compared to conventional approaches. The distinctive backbone structure of porphyrin, used as a building block to construct covalent organic frameworks (COFs), effectively modulates the aggregation of acoustic sensitizer molecules. COFs, when employed as acoustic sensitizers, exhibit a prolonged *in vivo* half-life in comparison to conventional small-molecule counterparts, facilitating enhanced penetration and tumor accumulation. In a groundbreaking study, Lu *et al.*[90] designed a COF-based acoustic sensitizer using porphyrin as a structural unit. This COF was efficiently loaded with a Toll-like receptor agonist (Poly(I:C))

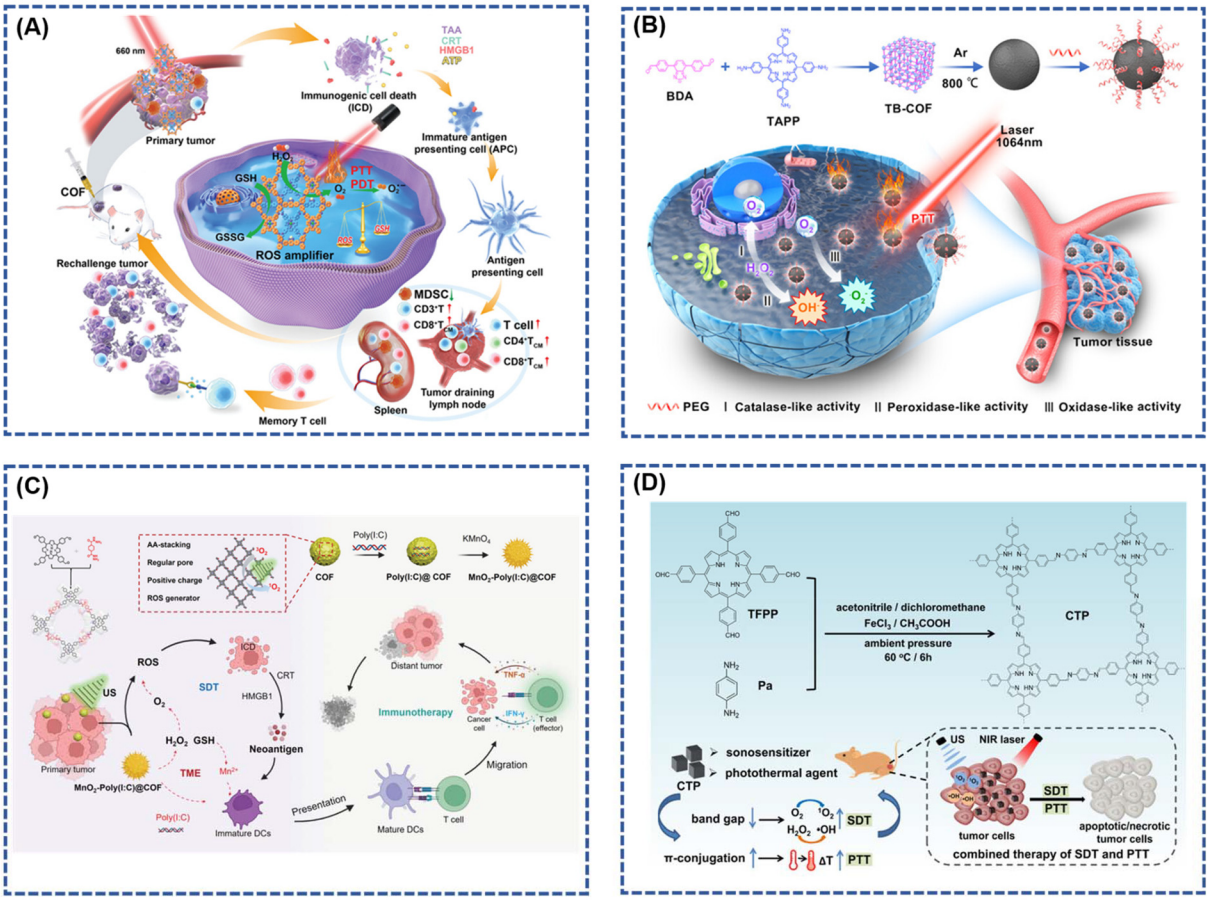

Fig. 8 (A) Illustration of the biological process and underlying mechanism of COF-618-Cu mediated PDT and PTT for triggering cancer immunotherapy; reproduced with permission of Ref. 26. Copyright © 2022, Zhang, Wiley. (B) Schematic illustration of the COF-Derived N-Doped Carbon Nanozyme with Multiple Enzyme-like Activities and Its Anticancer Mechanism; reproduced with permission of Ref. 89. Copyright © 2023, Wang, American Chemical Society. (C) Schematic illustration of the rational construction of MnO_2-Poly(I:C) @ COF NPs for enhanced sonodynamic therapy *via* remodeling tumor microenvironment and activating immune stimulation; reproduced with permission of Ref. 90. Copyright © 2022, Lu, Wiley. (D) Illustration of the Fabrication and Combined Therapy of CTP. Reproduced with permission of Ref. 91. Copyright © 2021, Liu, American Chemical Society.

and *in situ* grown paramagnetic transition metal oxide manganese dioxide (MnO_2). The synthesized MnO_2-Poly(I:C)@COF demonstrated superior capabilities in generating reactive oxygen species under ultrasound radiation and catalyzing the production of O2 from endogenous hydrogen peroxide (Fig. 8C). This enhancement in O_2-dependent SDT improved its acoustic sensitivity. Moreover, the tumor microenvironment's specificity promoted the release of Mn^{2+}, serving both as an excellent MRI contrast agent and, in tandem with Poly(I:C), significantly enhancing the dendritic cell's ability to present tumor antigens. This amplification facilitated cytotoxic T-cells' invasion into tumor tissues, bolstering the specific killing of tumor cells by these cells.

In another study, Liu *et al.*[91] reported the development of a cubic porphyrin-based covalent organic framework (COF) named CTP. This COF, synthesized using acetic acid and ferric chloride as catalysts, exhibited favorable hydrophilicity by attaching porphyrin monomers to carbon fibers through a simple and facile method. This approach overcame the challenges of poor solubility and biocompatibility associated with porphyrin monomers. Additionally, the formation of a π-conjugated structure narrowed the band gap, enabling effective photothermal conversion under external irradiation. Notably, CTP showed significantly improved solubility and acoustic kinetic effects compared to porphyrin monomers. The combined application of SDT and photothermal therapy (PTT) demonstrated positive therapeutic efficacy in breast cancer (Fig. 8D).

Exploiting the advantages of a three-dimensional covalent organic framework (3D COF) as an extended spatial network of molecular building blocks with numerous openings and active sites, Zhang *et al.*[92] developed a nanomaterial, 3D COF-TATB, embedded with copper ions (Cu^{2+}). In their photodynamic therapy system, Cu^{2+} complexed by the porphyrin photosensitizer within 3D COF-TATB was reduced by glutathione (GSH) to produce Cu^{+}, triggering a Fenton-like reaction that generated

hydroxyl radicals (–OH) and a single-linear state of oxygen ($^1O_2$). This cascade induced immunogenic cell death (ICD) in cancer cells (Fig. 9). The combination of 3D COF-TATB with an immune-blocking inhibitor (aPD-1), enhancing immunogenicity and activating the immune response against tumors, effectively inhibited tumor growth.

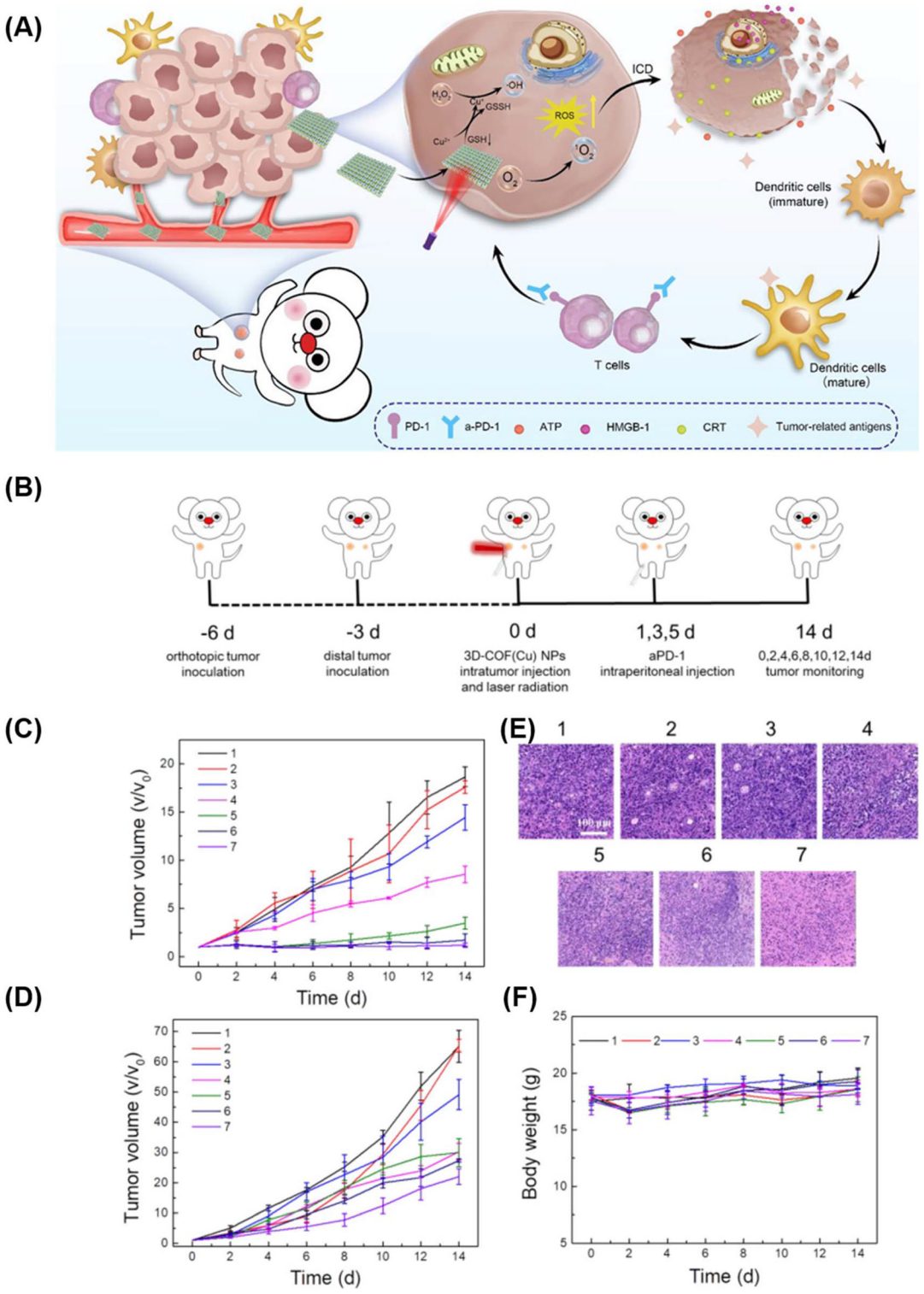

Fig. 9 (A) Schematic Illustration of 3D Cu@COF-TATB for Cancer Immunotherapy *via* PDT- and CDT-triggered ICD; (B) schematic diagram of the treatment process in mice. The volume curves of (C) primary tumor and (D) distant tumor. (E) H&E staining images of 4T1 tumor slides. (F) Body weights of 4T1 tumor-bearing mice with different treatments. Reproduced with permission of Ref. 92. Copyright © 2022, Zhang, American Chemical Society.

3.4. Photodynamic sterilization

Photodynamic Antimicrobial Therapy (PDAT) has become a focal point in the research landscape as a promising therapeutic strategy against bacterial diseases.[93–97] This approach offers notable advantages, including a reduction in therapeutic side effects and increased resilience against drug resistance—a critical concern in the field of bacterial infections.[95,98] The evolution of optical technology, coupled with the development of innovative photosensitizers, has propelled PDAT as a compelling solution for combating drug-resistant bacterial infections. In PDAT, photosensitizers, such as porphyrins, phthalides, and indocyanines, play a pivotal role by converting light energy into heat or reactive oxygen species (ROS), thereby inducing irreversible damage to bacteria.[96,99] The efficacy of photodynamic therapy (PDT) hinges on the concentration of photosensitizers at the lesion site. Achieving a high-density accumulation of these photosensitizers is imperative for eliciting a significant thermal effect and ensuring successful phototherapy.[97,100] Despite the potential of traditional photosensitizers, such as single freely available porphyrin molecules, their inherent self-aggregation-induced bursting poses a challenge, resulting in a drastic reduction in the effectiveness of PDT. This limitation has prompted the exploration of alternative solutions. In this context, covalent organic frameworks (COFs) built upon porphyrin molecules have emerged as robust photosensitizers for bacterial phototherapy. These COFs successfully overcome the self-aggregating nature that hampers the efficacy of individual porphyrin molecules.[101–103] The unique structure and properties of COFs based on porphyrins make them promising candidates for enhancing the photodynamic sterilization process, addressing the limitations associated with traditional photosensitizers and opening new avenues for advanced bacterial infection treatments.

In their study, Wang *et al.*[104] introduced the photosensitive unit TAPP and the reactive unit MMA-Da as monomers to synthesize multifunctional porphyrins (Por-COF) with high-activity double bonds and photosensitive capabilities through Schiff base condensation reactions (Fig. 10A). Employing a hydrothermal method, they integrated bacterial targeting with photothermal, photodynamic, and chemical sterilization, creating a Por-COF platform for synergistic phototherapy/chemotherapy. The Por-COF not only demonstrated enhanced bacterial capture by covalently binding to bacterial surface proteins *via* hyperactive surface double bonds but also efficiently eradicated bacteria through the generation of $^1O_2$ and hyperthermia *in situ*. *In vitro* and *in vivo* studies underscored its excellent cytocompatibility and negligible biotoxicity, emphasizing its potential for wound healing. Guern *et al.*[105] contributed a novel covalent compound featuring a cationic porphyrin covalently linked to a polymyxin B derivative (Fig. 10B). This peptide-coupled photosensitizer exhibited superior activity and targeting properties compared to commonly used cationic porphyrins. The Photoantimicrobial

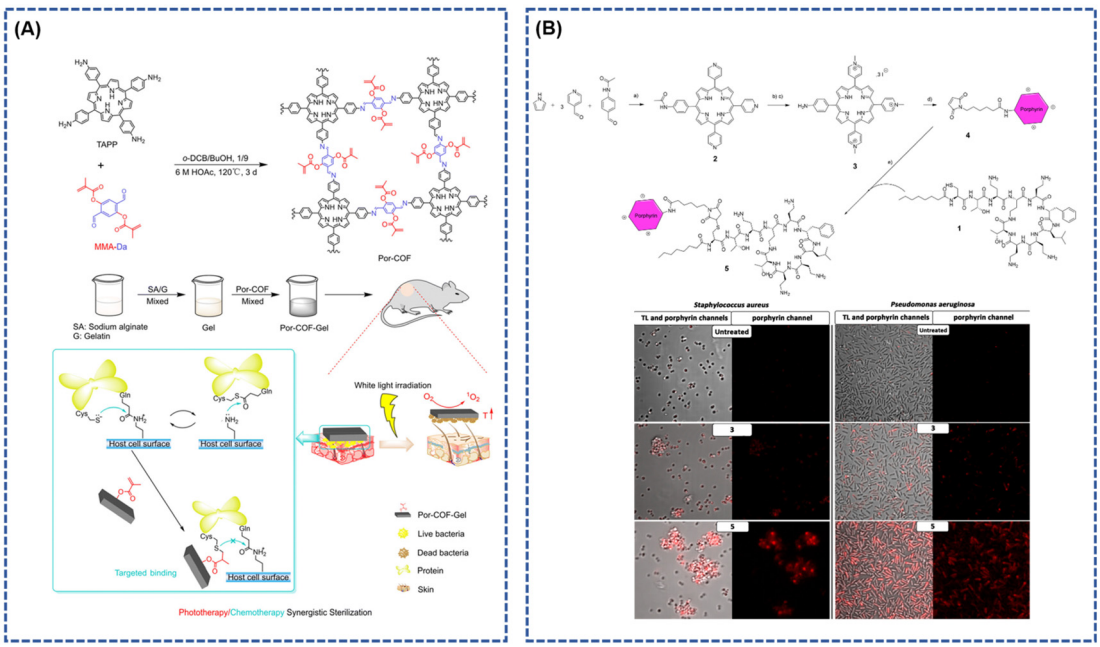

Fig. 10 (A) The design strategy and schematic of the Por-COF antibacterial nanoplatform; reproduced with permission of Ref. 104. Copyright © 2022, Wang, the Royal Society of Chemistry. (B) Synthetic Route of Cationic Porphyrin–Polymyxin B Conjugate (**5**)[a], Scheme (a) Propionic acid, 3 h, 140 °C. (b) Iodomethane, anhydrous dimethylformamide (DMF), 1 h, 140 °C. (c) 25% TFA/H_2O, 5 h, 100 °C. (d) 6-Maleimidohexanoic acid, HCTU, DIEA, anhydrous DMF, 24 h, RT. (e) PBS pH 6.5, 24 h, RT. And confocal laser scanning microscopy imaging of (left) *S. aureus* and (right) *P. aeruginosa* *in* different conditions: untreated and after incubation with **3** or **5**. Reproduced with permission of Ref. 105. Copyright © 2017, Guern, American Chemical Society.

Chemotherapy (PACT) efficiency was significantly enhanced, enabling selective adhesion to the cell walls of Gram-positive or Gram-negative bacteria and facilitating the generation of monoclinic oxygen. This targeted approach demonstrated efficacy against *Staphylococcus aureus*, *Pseudomonas aeruginosa*, and *Escherichia coli*.

Pathogenic microorganisms in environmental waters pose a significant threat to water quality, necessitating effective sterilization methods. Solar energy-based sterilization offers a promising and environmentally friendly approach, presenting considerable potential by reducing the energy consumption associated with conventional water treatment methods.[106] In a recent development, Wu *et al.*[107] demonstrated a novel synthesis where α-aminophosphonates were conjugated to p-COF through a three-component *in situ* one-pot Kabachnik field reaction (KF-3CR) at room temperature. The synthesis involved 5,10,15,20-tetrakis(4-aminophenyl) porphyrin (Tph), 2,5-dimethoxyterephthalaldehyde (DMTPA), and diethyl. By combining the resulting APCOF-1 with the environmentally friendly and cost-effective chitosan, a spiral device was fabricated, creating the APCOF-1@chitosan aerogel (Fig. 11A). This aerogel-based system demonstrated efficient sunlight-driven bacteriostasis in a continuous flow-passage water purifier model. Benefiting from the synergistic effects of bioactive α-aminophosphonate and photosensitive porphyrin within APCOF-1, the system exhibited an impressive solar-powered bactericidal efficacy of 97.1% against *Escherichia coli* (108 CFU mL^{-1}) in a 50 μL aqueous solution within a short timeframe of 90 minutes (Fig. 11B).

The transformation of powdered crystalline COFs into monolithic materials of diverse shapes, achieved through physical/chemical integration with flexible polymer matrices, *in situ* growth on organic/inorganic substrates, or interfacial polymerization, opens avenues for the creation of innovative and practical biomaterials boasting desired shapes and multiple therapeutic effects.[108,109] Ding *et al.*[80] made a notable contribution by reporting a homogeneous, self-supporting membrane based on porphyrin-covalent organic framework

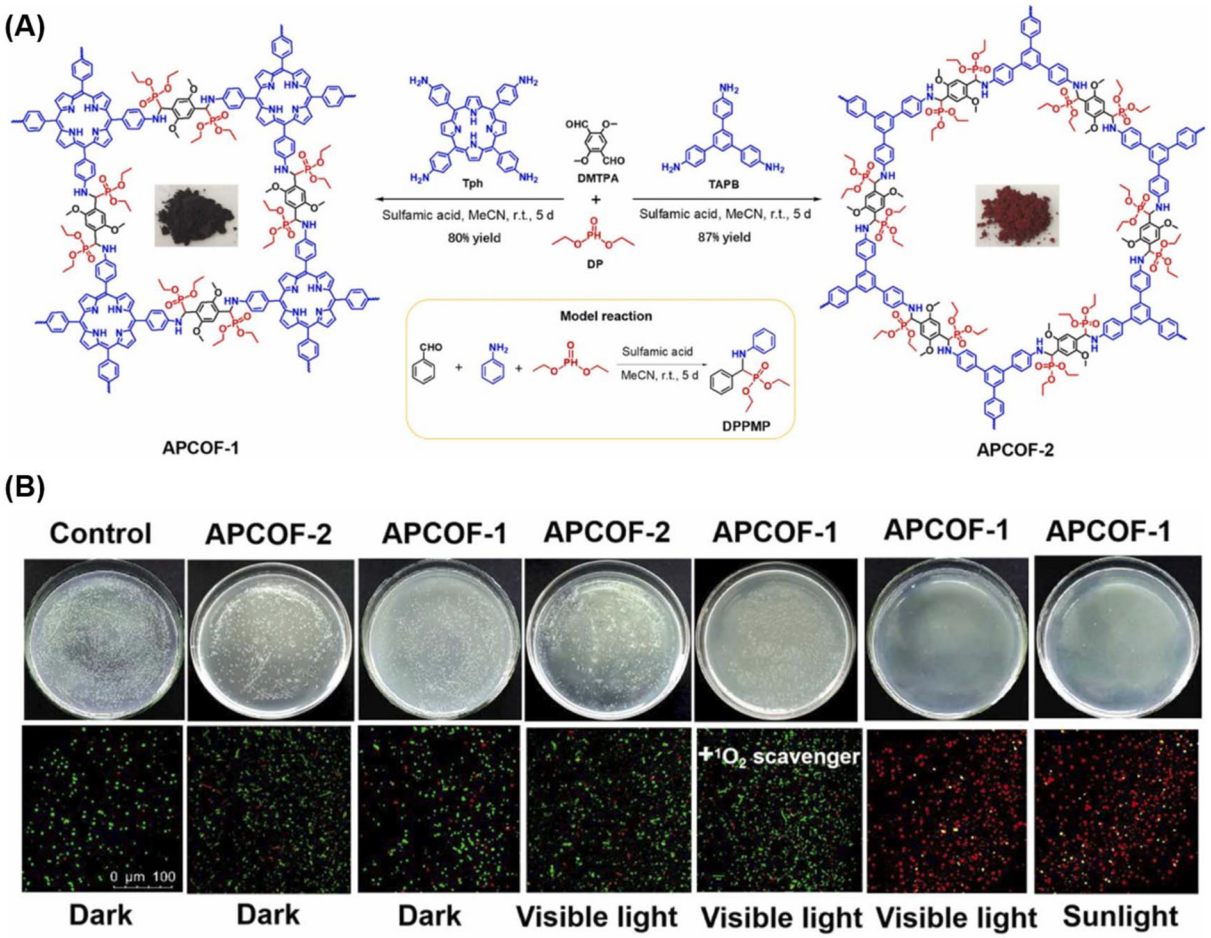

Fig. 11 (A) Synthesis of APCOF-1 and APCOF-2 *via* one-pot Kabachnik–Fields reaction at room temperature, with the corresponding photographs of COF samples and model reaction in the inset. (B) Photographs of bacteria culture plates and live/dead bacterial fluorescent images of different COF-treated groups against *E. coli* under different conditions (sample size: *d* = 9.0 cm). Reproduced with permission of Ref. 107. Copyright © 2022, Wu, Elsevier.

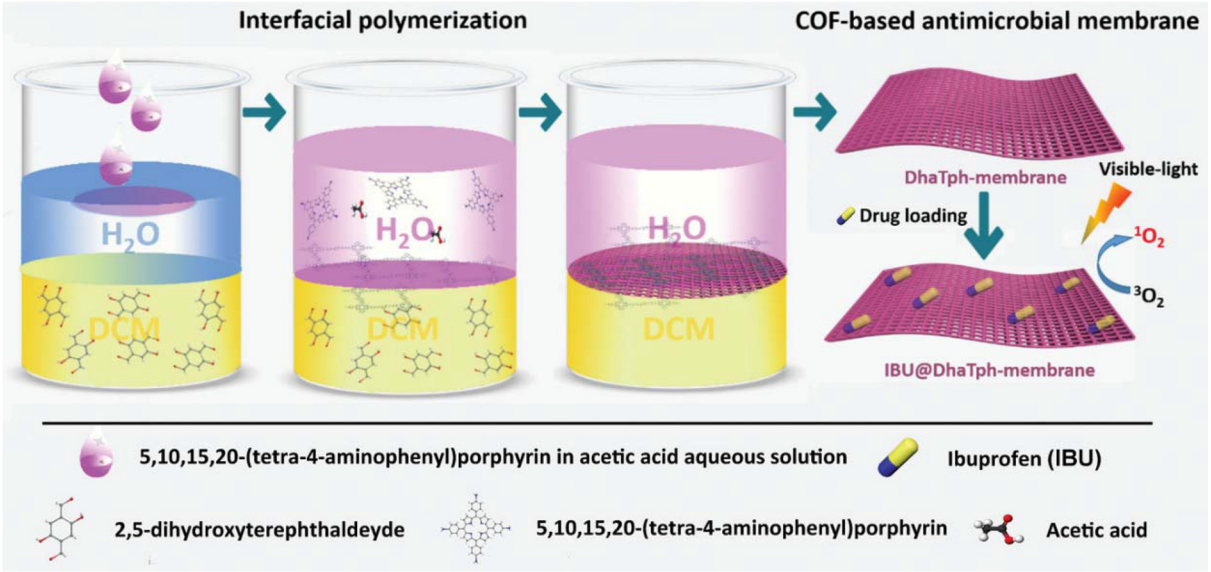

Fig. 12 Schematic illustration depicting the synthesis process of the multifunctional antimicrobial IBU@DhaTph-membrane. Reproduced with permission of Ref. 80. Copyright © 2021, Ding, Wiley.

(p-COF) containing encapsulated ibuprofen (IBU). *In vitro* experiments showcased the efficient antimicrobial and anti-inflammatory effects of the IBU@DhaTph-membranes, attributed to the synergistic light-induced generation of singlet oxygen ($^1O_2$) and controlled release of IBU (Fig. 12). Moreover, biocompatible "Band-Aid"-type dressings, utilizing IBU@DhaTph membranes, were prepared and demonstrated superior anti-infective and tissue remodeling activities in chronic wound healing assays conducted *in vivo*.

3.5. Drug delivery

Drug delivery involves the encapsulation or loading of therapeutic agents, particularly insoluble and unstable drugs, into nanocarriers for successful transport to the designated target. This approach mitigates systemic side effects, prolongs the half-life of free drugs, and enhances the efficacy of existing drugs.[13,110–112] Consequently, the development of drug delivery carriers with substantial surface area, high drug loading capacity, favorable biocompatibility, and multifunctional capabilities is imperative.[112,113] Covalent organic frameworks (COFs) stand out with their high surface area, porous structure, and favorable characteristics for achieving high drug loading capacity. COFs constructed with porphyrin and porphyrin derivatives as building blocks offer additional advantages, including low toxicity, excellent biodegradability, and minimal side effects on normal tissues, making them compelling candidates for drug delivery carriers.[114–118]

Gao *et al.*[119] introduced a covalent organic framework nanoparticle (COF NP) synthesized with porphyrin Tph and linker unit Dha as a carrier for the model drug doxorubicin (Dox). They designed an intelligent nano-system, TpDh-DT, based on these COFs (Fig. 13A). The nano-system utilized Cy5-labelled single-stranded DNA (ssDNA) for the recognition of covalent organic framework nanoparticles (COF NPs) loaded with Dox on the surface. The intra-pore-loaded Dox in COF NPs enhanced the interaction between COF and ssDNA, thereby improving the DNA loading density and fluorescence bursting efficiency to prevent drug leakage. This nano-system exhibited low fluorescent signals and reduced toxicity in normal cells. In contrast, in cancer cells, the overexpression of TK1 mRNA and the acidic microenvironment led to strong fluorescent signals and drug release. Luo *et al.*[116] prepared two porphyrin-based covalent triazine structures (PCTF and PCTF-Mn) *via* Friedel-Craft reaction under mild conditions. The field emission scanning electron microscope (FESEM) revealed irregular nanoparticles, while PCTF-Mn exhibited a plate-like morphology with desirable stability, large pore size, and high surface area. Drug release profiles determined by UV-vis spectrophotometry indicated similar release rates for the two PCTFs, with the majority of loaded IBUs released after 48 hours. The total releases reached 90% and 95% of the initial IBU loading, showcasing high-loading capacity and well-controlled release characteristics in the drug delivery assay.

In a recent development, Zhao *et al.*[114] presented a three-dimensional (3D) non-interpenetrating stp-topological porphyrin-based covalent organic framework (p-COF), denoted as TUS-64. This framework was synthesized *via* solvent pyrolysis of 5,10,15,20-tetrakis(4-aminophenyl) porphyrin (TAPP) and HFPTP as building blocks (in a 2 : 3 molar ratio) in an aqueous homo-xylene/1,4-dioxane/6 M acetic acid mixture (with a ratio of 7 : 3 : 1, v/v). TUS-64 exhibited remarkable thermochemical stability and a high specific surface area (Fig. 13B). Notably, TUS-64 demonstrated effective sustained drug delivery and precise site-specific targeted release of five distinct medications in a bodily fluid simulation, showcasing its relevance for drug delivery applications.[120]

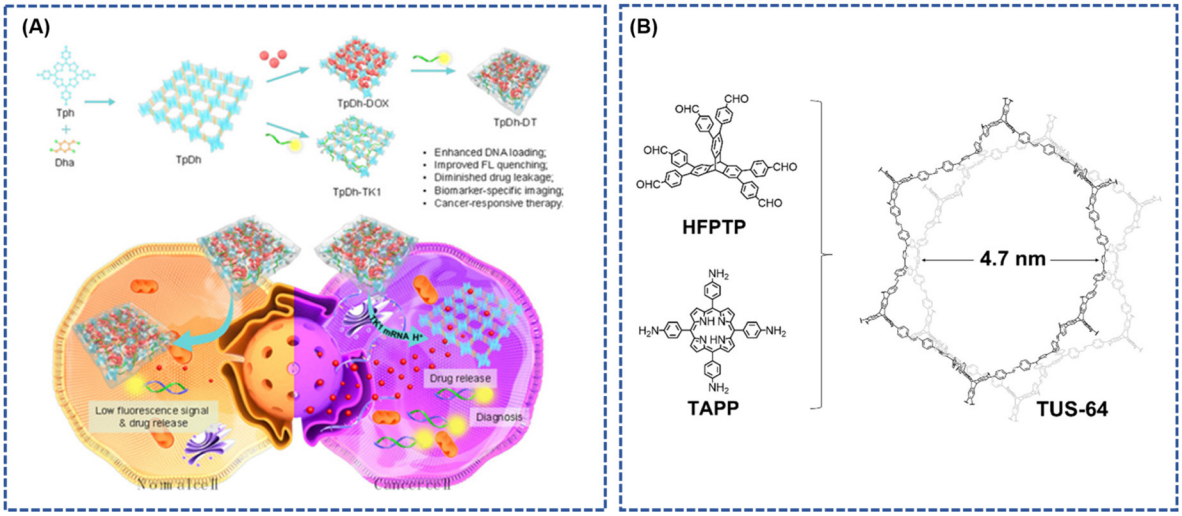

Fig. 13 (A) Schematic Illustration depicting the Preparation, Cancer Cell Specific Imaging, and Therapy Applications of TpDh-DT; reproduced with permission of Ref. 119. Copyright © 2021, Gao, American Chemical Society. (B) Conceptual representation elucidating the design of 3D TUS-64 with a noninterpenetrated stp net. Reproduced with permission of Ref. 114. Copyright © 2023, Zhao, Wiley.

4. Conclusions and perspectives

This review provides a deep exploration of the intricate realms of synthetic methodologies and the diverse spectrum of biological applications associated with porphyrin-based covalent organic frameworks (COFs). The integration of porphyrin molecules as fundamental building blocks within COFs emerges as a strategic solution, addressing the challenges posed by free-standing porphyrin molecules in practical biological applications. The unique planar conjugation and inherent biological properties of porphyrin molecules not only enhance COF stability but also introduce versatile functionalities, making them compelling materials for various biological applications. These COFs exhibit specific attributes such as a highly specific surface area, tunable pore structures, exceptional photosensitivity, and stability in both aqueous and chemical environments.

In the synthesis of porphyrin-based COFs, the chosen strategy significantly influences the material's performance in practical applications. Current synthesis methods often involve toxic catalysts, stringent conditions, and high temperatures, necessitating the development of greener, non-toxic synthetic methods for future research. The imperative lies in achieving controllability in the preparation of these materials to maximize their performance in practical applications. Despite the current emphasis on biosensors and biomimetic catalysis, there is a notable gap in exploring the potential of porphyrin-based COFs in cancer diagnosis, treatment, and drug transportation. Limited studies on toxicity warrant more in-depth investigations, while the inherent conductivity limitations of pure porphyrin-based COFs suggest exciting prospects in exploring composite materials for enhanced applications in diverse biological contexts.

The integration of machine-learning techniques holds immense promise in unraveling the intricate structure–property relationships inherent in porphyrin-based COFs and propelling the design of novel COFs with tailored functionalities. Machine learning offers a data-driven approach, enabling the extraction of complex patterns and correlations from vast datasets, particularly beneficial for understanding the multifaceted relationships between the structural attributes of porphyrin-based COFs and their resulting properties. Through advanced algorithms, machine learning facilitates the identification of critical features within the molecular framework, guiding the rational design of new porphyrin-based COFs with tailored functionalities. This synergy between machine learning and porphyrin-based COF research marks a paradigm shift in materials discovery and design, unlocking unprecedented opportunities for tailored materials with diverse applications in biological, catalytic, and sensing domains. As machine-learning techniques continue to evolve, their integration with porphyrin-based COF research is poised to revolutionize the discovery and design processes, ushering in a transformative era in materials science. The potential impact extends beyond the confines of current knowledge, paving the way for innovative materials that address complex challenges in biological applications.

Conflicts of interest

There are no conflicts to declare.

Acknowledgements

X.-G. Li thanks financial supports from The National Natural Science Foundation of China (52173011) and the Research and Development Project in Key Areas of Guangdong Province

(2023B0101020001). J. M. thanks financial supports from The National Natural Science Foundation of China (22276137), while J. Z. thanks financial supports from NSF (DMR-2311985) and ACS-PRF (ND-65277).

References

1 P. Kumari, N. Sinha, P. Chauhan and S. M. S. Chauhan, *Curr. Org. Synth.*, 2011, **8**, 393–437.
2 E. Sitte and M. O. Senge, *Eur. J. Org. Chem.*, 2020, **2020**, 3171–3191.
3 O. Koifman, T. Ageeva, I. Beletskaya, A. Averin, A. Yakushev, L. Tomilova, T. Dubinina, A. Tsivadze, Y. Gorbunova, A. Martynov, D. Konarev, S. Khasanov, R. Lyubovskaya, T. Lomova, V. Korolev, E. Zenkevich, T. Blaudeck, C. von Borczyskowski, D. Zahn, A. Mironov, N. Bragina, A. Ezhov, K. Zhdanova, P. Stuzhin, G. Pakhomov, N. Rusakova, N. Semenishyn, S. Smola, V. Parfenyuk, A. Vashurin, S. Makarov, I. Dereven'kov, N. Mamardashvili, T. Kurtikyan, G. Martirosyan, V. Burmistrov, V. Aleksandriiskii, I. Novikov, D. Pritmov, M. Grin, N. Suvorov, A. Tsigankov, A. Fedorov, N. Kuzmina, A. Nyuchev, V. Otvagin, A. Kustov, D. Belykh, D. Berezin, A. Solovieva, P. Timashev, E. Milaeva, Y. Gracheva, M. Dodokhova, A. Safronenko, D. Shpakovsky, S. Syrbu, Y. Gubarev, A. Kiselev, M. Koifman, N. Lebedeva and E. Yurina, *Macroheterocycles*, 2020, **13**, 311–467.
4 M. Faustova, E. Nikolskaya, M. Sokol, M. Fomicheva, R. Petrov and N. Yabbarov, *ACS Appl. Bio Mater.*, 2020, **3**, 8146–8171.
5 R. Chandra, M. Tiwari, P. Kaur, M. Sharma, R. Jain and S. Dass, *Indian J. Clin. Biochem.*, 2000, **15**, 183–199.
6 M. O. Senge, S. A. MacGowan and J. M. O'Brien, *Chem. Commun.*, 2015, **51**, 17031–17063.
7 M. O. Senge, *Chem. Commun.*, 2006, 243–256.
8 A. Martinez De Pinillos Bayona, P. Mroz, C. Thunshelle and M. Hamblin, *Chem. Biol. Drug Des.*, 2017, **89**, 192–206.
9 J. Dąbrowski, B. Pucelik, A. Regiel-Futyra, M. Brindell, O. Mazuryk, A. Kyzioł, G. Stochel, W. Macyk and L. Arnaut, *Coord. Chem. Rev.*, 2016, **325**, 67–101.
10 A. Aggarwal, N. Bhupathiraju, C. Farley and S. Singh, *Photochem. Photobiol.*, 2021, **97**, 1241–1265.
11 M. Imran, M. Ramzan, A. Qureshi, M. Khan and M. Tariq, *Biosensors*, 2018, **8**, 95–111.
12 M. Chou, H. Nalwa, N. Rakow and K. Suslick, *The Porphyrin Handbook*, 2000, 17263–17276.
13 S. Younis, D. Lim, K. Kim and A. Deep, *Adv. Colloid Interface Sci.*, 2020, **277**, 102108.
14 X. Zhao, L. Chen, K. Zhao, Y. Liu, J. Liu and X. Yan, *Trac-Trend. Anal. Chem.*, 2019, **5**, 65–72.
15 R. Liu, K. T. Tan, Y. Gong, Y. Chen, Z. Li, S. Xie, T. He, Z. Lu, H. Yang and D. Jiang, *Chem. Soc. Rev.*, 2021, **50**, 120–242.
16 W. Zhao, L. Xia and X. Liu, *CrystEngComm*, 2018, **20**, 1613–1634.
17 X. Liu, D. Huang, C. Lai, G. Zeng, L. Qin, H. Wang, H. Yi, B. Li, S. Liu, M. Zhang, R. Deng, Y. Fu, L. Li, W. Xue and S. Chen, *Chem. Soc. Rev.*, 2019, **48**, 5266–5302.
18 R. Sharma, P. Yadav, M. Yadav, R. Gupta, P. Rana, A. Srivastava, R. Zbořil, R. Varma, M. Antonietti and M. Gawande, *Mater. Horiz.*, 2020, **7**, 411–454.
19 D. Rodriguez-San-Miguel, C. Montoro and F. Zamora, *Chem. Soc. Rev.*, 2020, **49**, 2291–2302.
20 Q. Wang, L. Lv, W. Chi, Y. Bai, W. Gao, P. Zhu and J. Yu, *Biosensors*, 2023, **13**, 188–199.
21 J. Segura, S. Royuela and M. Mar Ramos, *Chem. Soc. Rev.*, 2019, **48**, 3903–3945.
22 N. Huang, P. Wang and D. Jiang, *Nat. Rev. Mater.*, 2016, **1**, 16068.
23 S. Qiao, M. Di, J.-X. Jiang and B.-H. Han, *EnergyChem*, 2022, **4**, 100094.
24 Y. Xie, M. Xu, L. Wang, H. Liang, L. Wang and Y. Song, *Mater. Sci. Eng., C*, 2020, **112**, 110864.
25 L. Zou, R. Sa, H. Lv, H. Zhong and R. Wang, *ChemSusChem*, 2020, **13**, 6124–6140.
26 L. Zhang, Y. Xiao, Q. C. Yang, L. L. Yang, S. C. Wan, S. Wang, L. Zhang, H. Deng and Z. J. Sun, *Adv. Funct. Mater.*, 2022, **32**, 2201542.
27 Y. Yusran, Q. Fang and V. Valtchev, *Adv. Mater.*, 2020, **32**, e2002038.
28 H. Lee, K. Hong and W. Jang, *Coord. Chem. Rev.*, 2018, **354**, 46–73.
29 M. Chen, H. Li, C. Liu, J. Liu, Y. Feng, A. G. H. Wee and B. Zhang, *Coord. Chem. Rev.*, 2021, **435**, 213778.
30 S. Huang, K. Chen and T. Li, *Coord. Chem. Rev.*, 2022, **464**, 214563.
31 S. Rowan, S. Cantrill, G. Cousins, J. Sanders and J. Stoddart, *Angew. Chem., Int. Ed.*, 2002, **41**, 898–952.
32 J. Wang and S. Zhuang, *Coord. Chem. Rev.*, 2019, **400**, 213046.
33 J. Tang, Z. Liang, H. Qin, X. Liu, B. Zhai, Z. Su, Q. Liu, H. Lei, K. Liu, C. Zhao, R. Cao and Y. Fang, *Angew. Chem., Int. Ed.*, 2023, **62**, e202214449.
34 M. S. Lohse and T. Bein, *Adv. Funct. Mater.*, 2018, **28**, 1705553.
35 T. Skorjanc, D. Shetty and A. Trabolsi, *Chem*, 2021, **7**, 882–918.
36 X. Chen, M. Addicoat, E. Jin, H. Xu, T. Hayashi, F. Xu, N. Huang, S. Irle and D. Jiang, *Sci. Rep.*, 2015, **5**, 14650.
37 A. Nagai, X. Chen, X. Feng, X. Ding, Z. Guo and D. Jiang, *Angew. Chem., Int. Ed.*, 2013, **52**, 3770–3774.
38 B. Nath, W.-H. Li, J.-H. Huang, G.-E. Wang, Z.-h. Fu, M.-S. Yao and G. Xu, *CrystEngComm*, 2016, **18**, 4259–4263.
39 R. Chen, J. L. Shi, Y. Ma, G. Lin, X. Lang and C. Wang, *Angew. Chem., Int. Ed.*, 2019, **58**, 6430–6434.
40 X. Chen, M. Addicoat, S. Irle, A. Nagai and D. Jiang, *J. Am. Chem. Soc.*, 2012, **135**, 546–549.
41 X. Chen, M. Addicoat, E. Jin, L. Zhai, H. Xu, N. Huang, Z. Guo, L. Liu, S. Irle and D. Jiang, *J. Am. Chem. Soc.*, 2015, **137**, 3241–3247.

42 S. Kandambeth, D. B. Shinde, M. K. Panda, B. Lukose, T. Heine and R. Banerjee, *Angew. Chem., Int. Ed.*, 2013, **52**, 13052–13056.
43 M. Zhang, J.-P. Liao, R.-H. Li, S.-N. Sun, M. Lu, L.-Z. Dong, P. Huang, S.-L. Li, Y.-P. Cai and Y.-Q. Lan, *Natl. Sci. Rev.*, 2023, **10**, 1093.
44 Y. Yue, P. Cai, K. Xu, H. Li, H. Chen, H.-C. Zhou and N. Huang, *J. Am. Chem. Soc.*, 2021, **143**, 18052–18060.
45 S. Daliran, M. Blanco, A. Dhakshinamoorthy, A. R. Oveisi, J. Alemán and H. García, *Adv. Funct. Mater.*, 2023, **34**, 2312912.
46 X. Xu and J. Moulijn, *Energy Fuels*, 1996, **10**, 305–325.
47 R. Grim, Z. Huang, M. Guarnieri, J. Ferrell, L. Tao and J. Schaidle, *Energy Environ. Sci.*, 2020, **13**, 472–494.
48 J. Artz, T. E. Müller, K. Thenert, J. Kleinekorte, R. Meys, A. Sternberg, A. Bardow and W. Leitner, *Chem. Rev.*, 2017, **118**, 434–504.
49 Q. Fan, M. Zhang, M. Jia, S. Liu, J. Qiu and Z. Sun, *Mater. Today Energy*, 2018, **10**, 280–301.
50 C. Xiao and J. Zhang, *ACS Nano*, 2021, **15**, 7975–8000.
51 S. Jin, Z. Hao, K. Zhang, Z. Yan and J. Chen, *Angew. Chem., Int. Ed.*, 2021, **60**, 20627–20648.
52 Q. Lu and F. Jiao, *Nano Energy*, 2016, **29**, 439–456.
53 X. Cui, S. Lei, A. C. Wang, L. Gao, Q. Zhang, Y. Yang and Z. Lin, *Nano Energy*, 2020, **70**, 10525.
54 Z. Liang, H. Y. Wang, H. Zheng, W. Zhang and R. Cao, *Chem. Soc. Rev.*, 2021, **50**, 2540–2581.
55 Y. Wang, H. Ding, X. Ma, M. Liu, Y. Yang, Y. Chen, S. Li and Y. Lan, *Angew. Chem., Int. Ed.*, 2021, **61**, 2114648.
56 L. Gong, B. Chen, Y. Gao, B. Yu, Y. Wang, B. Han, C. Lin, Y. Bian, D. Qi and J. Jiang, *Inorg. Chem. Front.*, 2022, **9**, 3217–3223.
57 Z. Ren, B. Zhao and J. Xie, *Small*, 2023, **19**, e2301818.
58 X. Yang, J. Cheng, X. Xuan, N. Liu and J. Liu, *ACS Sustainable Chem. Eng.*, 2020, **8**, 10536–10543.
59 G. Zhou, L. Zhang, Y. Xia, H. Xu, W. Yin, S. Wang, J. Yi, X. Zhu, X. Ning and X. Wang, *Chem. Eng. J.*, 2023, **477**, 147040.
60 H. Choi, D.-K. Lee, M.-K. Han, G. Janani, S. Surendran, J. H. Kim, J. K. Kim, H. Cho and U. Sim, *J. Electrochem. Soc.*, 2020, **167**, 164503.
61 Y. Bai, W. Gao, Q. Wang, B. Yu, J. Wei, C. Gao, P. Zhu and J. Yu, *Sens. Actuators, B*, 2023, **394**, 134435.
62 Y. Yuan, K. T. Bang, R. Wang and Y. Kim, *Adv. Mater.*, 2023, **35**, 2210952.
63 Y.-C. Feng, X. Wang and D. Wang, *Mater. Chem. Front.*, 2024, **8**, 228–247.
64 J. Tang, C. Su and Z. Shao, *Small Methods*, 2021, **5**, 2100945.
65 S. An, C. Lu, Q. Xu, C. Lian, C. Peng, J. Hu, X. Zhuang and H. Liu, *ACS Energy Lett.*, 2021, **6**, 3496–3502.
66 Y.-N. Gong, W. Zhong, Y. Li, Y. Qiu, L. Zheng, J. Jiang and H.-L. Jiang, *J. Am. Chem. Soc.*, 2020, **142**, 16723–16731.
67 Y. Zhu, D. Zhu, Y. Chen, Q. Yan, C.-Y. Liu, K. Ling, Y. Liu, D. Lee, X. Wu, T. P. Senftle and R. Verduzco, *Chem. Sci.*, 2021, **12**, 16092–16099.
68 C. Jin, N. Li, E. Lin, X. Chen, T. Wang, Y. Wang, M. Yang, W. Liu, J. Yu, Z. Zhang and Y. Chen, *ACS Catal.*, 2022, **12**, 8259–8268.
69 A. Mushtaq, R. Fatima, F. K. Shehzad, M. Ammar, I. A. Shaaban, M. A. Assiri, M. Sajid, H. M. Asif and S. Hussain, *Inorg. Chim. Acta*, 2023, **558**, 121745.
70 X. Liu, R. Qi, S. Li, W. Liu, Y. Yu, J. Wang, S. Wu, K. Ding and Y. Yu, *J. Am. Chem. Soc.*, 2022, **144**, 23396–23404.
71 L. Jin, S. Lv, Y. Miao, D. Liu and F. Song, *ChemCatChem*, 2020, **13**, 140–152.
72 Z. Lu, H. Yang, X. Fu, Y. Zhao, Q. Lin, L. Xiao and L. Hou, *Mater. Today Chem.*, 2022, **25**, 2291–2298.
73 J. Shu and D. Tang, *Anal. Chem.*, 2019, **92**, 363–377.
74 Z. Qiu and D. Tang, *J. Mater. Chem. B*, 2020, **8**, 2541–2561.
75 S. Bayda, E. Amadio, S. Cailotto, Y. Frión-Herrera, A. Perosa and F. Rizzolio, *Nanoscale Adv.*, 2021, **3**, 5183–5221.
76 C. Tan, X. Cao, X.-J. Wu, Q. He, J. Yang, X. Zhang, J. Chen, W. Zhao, S. Han, G.-H. Nam, M. Sindoro and H. Zhang, *Chem. Rev.*, 2017, **117**, 6225–6331.
77 J. Cui, Y. Zhang, K. Lun, B. Wu, L. He, M. Wang, S. Fang, Z. Zhang and L. Zhou, *Microchim. Acta*, 2023, **190**, 23421.
78 X. Wang, C. Hou, F. Zhang, J. Xia and Z. Wang, *Sens. Actuators, B*, 2023, **379**, 133229.
79 J. Cui, L. Kan, Z. Li, L. Yang, M. Wang, L. He, Y. Lou, Y. Xue and Z. Zhang, *Talanta*, 2021, **228**, 122060.
80 L. Ding, S. Wang, B. Yao, F. Li, Y. Li, G. Zhao and Y. Dong, *J. Mater. Chem. A*, 2021, **10**, 3346–3358.
81 S. Patial, V. Soni, A. Kumar, P. Raizada, T. Ahamad, X. Pham, Q. Le, V. Nguyen, S. Thakur and P. Singh, *Coord. Chem. Rev.*, 2022, **452**, 214298.
82 X. Wang, L. Li, D. Li and J. Ye, *Sol. RRL*, 2020, **4**, 200574.
83 X. Zhang, K.-N. Chi, D.-L. Li, Y. Deng, Y.-C. Ma, Q.-Q. Xu, R. Hu and Y.-H. Yang, *Biosens. Bioelectron.*, 2019, **129**, 64–71.
84 Z. Zheng, L. Ma, B. Li and X. Zhang, *Anal. Chem.*, 2023, **95**, 13855–13863.
85 P. Zhu, S. Li, S. Zhou, N. Ren, S. Ge, Y. Zhang, Y. Wang and J. Yu, *Chem. Eng. J.*, 2021, **420**, 127559.
86 X. Yan, Y. Song, J. Liu, N. Zhou, C. Zhang, L. He, Z. Zhang and Z. Liu, *Biosens. Bioelectron.*, 2019, **126**, 734–742.
87 S. Yao, Z. Liu and L. Li, *Nano-Micro Lett.*, 2021, **13**, 176.
88 P. Gao, X. Shen, X. Liu, B. Cui, M. Wang, X. Wan, N. Li and B. Tang, *ACS Appl. Mater. Interfaces*, 2021, **13**, 41498–41506.
89 X. Wan, Y. Ge, J. Zhang, W. Pan, N. Li and B. Tang, *ACS Appl. Mater. Interfaces*, 2023, **15**, 44763–44772.
90 Z. Lu, S. Bai, Y. Jiang, S. Wu, D. Xu, Y. Chen, Y. Lan, Y. An, J. Mao, X. Liu and G. Liu, *Adv. Funct. Mater.*, 2022, **32**, 2207749.
91 S. Liu, Z. Liu, Q. Meng, C. Chen and M. Pang, *ACS Appl. Mater. Interfaces*, 2021, **13**, 56873–56880.
92 X. Zhang, S. Wang, K. Tang, W. Pan, H. Xu, Y. Li, Y. Gao, N. Li and B. Tang, *ACS Appl. Mater. Interfaces*, 2022, **14**, 30618–30625.
93 S. S. Lucky, K. C. Soo and Y. Zhang, *Chem. Rev.*, 2015, **115**, 1990–2042.
94 T. C. Pham, V.-N. Nguyen, Y. Choi, S. Lee and J. Yoon, *Chem. Rev.*, 2021, **121**, 13454–13619.

95 A. P. Castano, T. N. Demidova and M. R. Hamblin, *Photodiagn. Photodyn. Ther.*, 2005, **2**, 91–106.
96 J. Chen, T. Fan, Z. Xie, Q. Zeng, P. Xue, T. Zheng, Y. Chen, X. Luo and H. Zhang, *Biomaterials*, 2020, **237**, 119827.
97 K. Deng, C. Li, S. Huang, B. Xing, D. Jin, Q. Zeng, Z. Hou and J. Lin, *Small*, 2017, **13**, 1702299.
98 J. H. Correia, J. A. Rodrigues, S. Pimenta, T. Dong and Z. Yang, *Pharmaceutics*, 2021, **13**, 1332.
99 D. Straten, V. Mashayekhi, H. de Bruijn, S. Oliveira and D. Robinson, *Cancers*, 2017, **9**, 20019.
100 R. Allison and K. Moghissi, *Photodiagn. Photodyn. Ther.*, 2013, **10**, 331–341.
101 I. Mavridis and K. Yannakopoulou, *J. Med. Chem.*, 2019, **63**, 3391–3424.
102 X. Xing, S. Zhao, T. Xu, L. Huang, Y. Zhang, M. Lan, C. Lin, X. Zheng and P. Wang, *Coord. Chem. Rev.*, 2021, **445**, 214087.
103 D. Gao, X. Guo, X. Zhang, S. Chen, Y. Wang, T. Chen, G. Huang, Y. Gao, Z. Tian and Z. Yang, *Mater. Today Bio*, 2020, **5**, 100035.
104 M.-C. Wang, J.-X. Guo, L.-J. Chen and X. Zhao, *Biomater. Sci.*, 2023, **11**, 1776–1784.
105 F. Le Guern, V. Sol, C. Ouk, P. Arnoux, C. Frochot and T.-S. Ouk, *Bioconjugate Chem.*, 2017, **28**, 2493–2506.
106 J. Cabral, *Int. J. Environ. Res. Public Health*, 2010, **7**, 3657–3703.
107 W. Wu, F. Li, B. Yao, L. Ding, J. Kan, F. Liu, G. Zhao, S. Wang and Y. Dong, *J. Hazard. Mater.*, 2022, **433**, 128831.
108 A. Matthieu Weber, A. Ayral, P. Miele and M. Bechelany, *Chem. Mater.*, 2018, **30**, 7368–7390.
109 A. Tripathi and J. Bonilla-Cruz, *ACS Appl. Nano Mater.*, 2023, **6**, 5042–5074.
110 L. Bai, S. Z. F. Phua, W. Q. Lim, A. Jana, Z. Luo, H. P. Tham, L. Zhao, Q. Gao and Y. Zhao, *Chem. Commun.*, 2016, **52**, 4128–4131.
111 H. Guo, Y. Liu, N. Wu, L. Sun and W. Yang, *ChemistrySelect*, 2022, **7**, 2202538.
112 M. C. Scicluna and L. Vella-Zarb, *ACS Appl. Nano Mater.*, 2020, **3**, 3097–3115.
113 K. Bera, S. Maiti, M. Maity, C. Mandal and N. C. Maiti, *ACS Omega*, 2018, **3**, 4602–4619.
114 Y. Zhao, S. Das, T. Sekine, H. Mabuchi, T. Irie, J. Sakai, D. Wen, W. Zhu, T. Ben and Y. Negishi, *Angew. Chem., Int. Ed.*, 2023, **62**, 2300172.
115 M.-X. Wu and Y.-W. Yang, *Chin. Chem. Lett.*, 2017, **28**, 1135–1143.
116 Y. Luo, J. Liu, Y. Liu and Y. Lyu, *J. Polym. Sci., Part A: Polym. Chem.*, 2017, **55**, 2594–2600.
117 P. Ghosh and P. Banerjee, *Chem. Commun.*, 2023, **59**, 12527–12547.
118 N. Singh, S. Son, J. An, I. Kim, M. Choi, N. Kong, W. Tao and J. S. Kim, *Chem. Soc. Rev.*, 2021, **50**, 12883–12896.
119 P. Gao, X. Shen, X. Liu, Y. Chen, W. Pan, N. Li and B. Tang, *Anal. Chem.*, 2021, **93**, 11751–11757.
120 G. Lin, H. Ding, R. Chen, Z. Peng, B. Wang and C. Wang, *J. Am. Chem. Soc.*, 2017, **139**, 8705–8709.